MSc thesis in Geomatics

# The effects of beach house configurations on dune-ward sediment transport

Anna Vera Stevers

TU Delft

MSc thesis in Geomatics

# The effects of beach house configurations on dune-ward sediment transport

Anna Vera Stevers

June 2021

A thesis submitted to the Delft University of Technology in partial fulfilment of the requirements for the degree of Master of Science in Geomatics

An electronic version of this thesis is available at: http://repository.tudelft.nl/
Cover image by: Andy Troy. Image is retrieved from: https://andytroy.nl/wp-content/uploads/2017/04/1303-vrouwenpolder-44_3_5.jpg

The work in this thesis was carried out in the:


3D geoinformation group
Delft University of Technology

Supervisors: Dr. Clara García-Sánchez
Dr. Giorgio Agugiaro
Ivan Pađen
Co-reader: Dr.ir. Marjolein Pijpers-van Esch

# Abstract

In the Netherlands, the coastal dunes are essential to protect the country against flooding. However, the rising sea levels increase the risk of flooding along these sandy shores. Moreover, due to a combination of human and natural activities, dune erosion has increased and will continue to do so in the coming decades. Besides flood protection, the Dutch shoreline is important for preserving biodiversity, the generation of drinking water and recreation. In recent year, the number of recreational buildings on the beach, such as bars and holiday homes has increased. This is relevant because previous studies show that such beach buildings affect the wind flow and limit aeolian transport of sediment towards the dunes.

This research studies the impact of beach house configurations on dune-ward sediment transport to limit the adverse effects on dune development. We use CFD simulations to study the wind flow around a 3D model of a beach with holiday houses, based on a section of the Noordwijk beach in the Netherlands. We implement the CFD software OpenFOAM to solve the RANS equations for turbulent, steady-state flow. The sediment transport that occurs is calculated using the wind direction and speed near the ground surface of the solution.

The study consists of multiple 3D models in which the placement of the houses is varied systematically, to study the effects of beach house configurations. Variations are made by rotating houses, individually or within a row, and changing the distance between the houses and dunes. We determine the annual effect on sediment transport by applying varying wind conditions based on historical wind data from Noordwijk. As we have many simulations to run, and all need different parameters and settings, we automated the process. First, a PostgreSQL database is used to store all requirements for the CFD simulations, the metadata and the results the simulations give. Then, a Python script links the information stored in the database to the correct settings in OpenFOAM. This way, many simulations are run in a row, and the results area to compare.

The results show that rotating the houses individually towards the prevailing wind direction appears to improve the amount of dune-ward sediment that takes place, compared to beach houses placed perpendicular to the shore. Rotating a row of houses as a whole has a limited effect on the amount of sediment transport. However, combining the rotation of the row of houses and the houses individually towards the prevailing wind direction shows the best improvement in sediment transport. Changing the distance between the houses and the dune foot so that a row of houses forms a funnel shape pointing towards the dunes also yields promising results. Because we use a simplified model and do not take factors such as moisture levels or fetch distance into account, the results of this study overestimate the amount of sediment transport that takes place and might not quite resemble the reality. Further research using scale models or wind tunnels is necessary to confirm the suggestions made in this thesis.

# Acknowledgements

When I started working on this thesis nearly a year ago, I had hardly heard of CFD before and had only a little experience working with databases. Those people who know me well know I like to be challenged and can be very stubborn, although in my c.v. I would describe this as perseverance. This meant that, although knowing very little about CFD and feeling somewhat overwhelmed, I dove deep into the topic and would not let go. It sure was a steep learning curve in the first couple of months. Looking back now, I have learned a lot and achieved more than I thought I could all these months ago. I could not have achieved these results all by myself.

Therefore, I would like to thank my TU Delft supervisors, Clara García-Sánchez, for her guidance and help with all CFD related problems, and Giorgio Agugiaro, for the support on database management and reassurance whenever I felt unsure. Many thanks also to Ivan Pađen, who stepped in as substitute supervisor whenever necessary and the co-reader Marjolein Pijpers-van Esh for her constructive feedback. Furthermore, I wish to express my gratitude to the researchers from ShoreScape, particularly Janneke van Bergen, who provided me with the necessary input data and helped me when necessary. I should also mention Nadine Hobeika, to whom I have asked a thousand questions and who was a great companion during this research. Lastly, thanks to my family, friends and Maarten, for keeping me sane and providing me with chocolate, cups of tea and distracting (beach) walks.

# Contents

# List of Figures

# List of Tables

# Acronyms

# Nomenclature

| | | |
|---|---|---|
| $\kappa$ | Von Kármán's constant = 0.42 | |
| $\rho_a$ | Air density | $kgm^{-3}$ |
| $\rho_s$ | Sand density | $kgm^{-3}$ |
| $\varepsilon$ | turbulence dissipation rate | $m^2s^{-3}$ |
| $A$ | Coefficient depending on particle friction = 0.1 | |
| $C_\mu$ | Model constant = 0.09 | |
| $C_B$ | Bagnold's empirical coefficient = 1.8 | |
| $D$ | Reference grain diameter = 0.25 | $m$ |
| $d$ | Median grain size | $m$ |
| $g$ | Gravitational acceleration = 9.81 | $ms^{-2}$ |
| $k$ | Turbulent kinetic energy | $m^2s^{-2}$ |
| $q$ | Sediment transport | $kgm^{-1}s^{-1}$ |
| $Q_D$ | Dune-wards sediment transport | $kgm^{-1}s^{-1}$ |
| $U(z)$ | Wind speed at elevation z | $ms^{-1}$ |
| $u_*$ | Shear velocity | $ms^{-1}$ |
| $y^+$ | Dimensionless wall unit describing the distance from a point to a wall | |
| $z_0$ | Aerodynamic roughness length | $m$ |

# 1 Introduction

## 1.1 Background

As the sea levels rise due to climate change, coastal areas are at increased risk of flooding (Stronkhorst et al., 2018). In the Netherlands, where large parts of coastal areas are urbanised and most of the population lives below sea level, flood control is a serious issue. Along the Dutch sandy shores, the dunes are the first line of defence against the rising sea. The natural development of these dunes is a dynamic process of erosion and accretion (Nordstrom & Jackson, 2013).

However, in recent years the amount of dune erosion has increased (L. van Rijn, 2011). The increase in dune erosion is partly due to the consequences of climate change, such as an increase in strong winds (de Winter & Ruessink, 2017). On the other hand, a fundamental part of erosion can be attributed to human activities. Currently, the dunes are maintained using artificial sand nourishments where sand is deposited in the sea near the shore. These nourishments rely on wind-driven sediment transport to bring the sand inland to the dunes. Along many of the Netherlands' beaches, there is a growing number of beach houses and recreational buildings. These buildings generally limit the amount of aeolian sediment transport towards the dunes (Hoonhout & van Thiel de Vries, 2013; Jackson & Nordstrom, 2011). The arrangements in which the beach houses are placed appear to affect the sediment transport that could take place (van Onselen, 2018; van Westen, 2019).

Previous studies have looked at the influence of beach houses on sediment transport by studying scale models, satellite images or taking on-site measurements. van Onselen (2018) was one of the first to use computer-generated models to study the impact of beach houses on sediment transport. In his work, he simulated different beach house arrangements to see how they affect sediment transport differently. This thesis continues his research by changing the beach house arrangements and taking different wind conditions into account.

Using computational fluid dynamics (CFD) models, we have the opportunity to test many different beach house configurations rapidly. Additionally, by simulating scenarios with varying wind conditions, we can predict the long term variation in sediment flow. Comparing these simulations shows the differences between several beach house configurations on the sediment transport. This could show how the beach houses can be placed to let sediment transport happen as naturally as possible. Furthermore, we can look at the possibility to increase sediment transport locally and aid in dune formation.

### 1.1.1 Shorescape

This thesis is written in collaboration with ShoreScape, an interdisciplinary research project conducted by the TU Delft and the University of Twente. The project's purpose is to design a sustainable coastal zone along sandy shores. They aim to ensure coastal protection and allow space for recreation, but not at the expense of the natural environment in the dunes. One of their specific goals is to use natural landscaping mechanisms to improve dune formation (van Bergen & Nijhuis, 2019).

As part of the project, van Bergen et al. (2021) did several real-life field experiments in 2019 using scale models (figure 1.1). To get better insights into the effects of beach houses on beach and dune development. These first

field experiments were conducted using the promising results from van Onselen (2018)). The results from this thesis will advise ShoreScape further on the effects of different configurations. If the results look promising, some of the beach house configurations can be tested as scale models on beaches later in 2021.

**Figure 1.1.** Scale models on beach of Scheveningen (van Bergen et al., 2021)

## 1.2 Problem statement

To summarise shortly, due to both human and natural activities, the amount of dune erosion is increasing. Beach houses play a role in the sediment transport from the sea to the beach. Therefore, it is important to know how the beach houses can limit the sediment transport the least, or perhaps even locally increase the transport. Previous studies show that changing the arrangements in which the beach houses are placed can impact sediment transport. However, more results are necessary, using different beach house arrangements and incoming wind conditions.

## 1.3 Aim and objectives

This thesis aims to model different types of beach house configurations and the effects these have on the wind blowing around these houses. Using the modelled effects on the wind, we aim to estimate the dune-ward sediment flow in every configuration. Comparing the results of different configurations can tell us more about the potential factors that limit dune-ward sediment flow.

To achieve these aims, we use a case study of the beach of Noordwijk, a town in the Netherlands. 3D models are made for a section of this beach with different beach house configurations. The effects of the wind around the 3D models can be simulated by creating CFD models using Open-source Field Operation And Manipulation (OpenFOAM) software. The simulations show the direction and speed of the wind around the 3D models. The simulations use multiple wind directions and speeds to give accurate and long-term results. The wind directions and wind speeds are based on actual wind data from Noordwijk to make it as realistic as possible. An estimated amount of sediment transport can be determined based on the wind simulations. Furthermore, looking specifically at the wind direction and sediment transport, we can predict the amount of sediment transport going towards the dunes. These approximations can be used to determine what the effects of the different configurations are on dune-ward sediment transport.

Secondly, another aim is to store the data of the different scenarios in an efficient way. This also makes it easy to compare scenarios with each other. Little is known about how other studies did this previously. Therefore we aim to set up an easy to use database system. The added value of a database is, first and foremost, that it is an efficient way to store large amounts of data. Furthermore, it would aid in the comparison between scenarios as all the necessary data is stored in one centralised, shared place and easy to retrieve. Lastly, it is a way to share the results from the different simulation with others easily.

## 1.4 Research questions

The aims are achievable by answering the following research question:

**What are the effects of different beach house configurations on dune-ward sediment transport?**

The following sub-questions are relevant to answer the main research question:

- What are the effects of the changing seasonal wind conditions on dune-wards sediment transport according to CFD simulations?
- How do different beach house configurations compare in regards to dune-ward sediment transport?
- What are the potential effects of beach house configurations on sedimentation and dune formation?

## 1.5 Report structure

The report starts with a chapter on context of the dunes, which explains the processes involved, such as dune development, sediment transport and dune management by the government. The third chapter consists of a theoretical framework behind running CFD simulations. Chapter four explain the methodology we used to run CFD simulations, including the pre-and post-processing. The fifth chapter continues with implementing a database and the methodology behind automation and running multiple simulations in a row. In chapter six, the results are presented. Beginning with comparing sediment transport on an empty beach to sediment transport on a beach with houses. The chapter continues by comparing the effects of changing wind conditions and of different beach house configurations. The chapter finishes with a comparison of the results of all configurations. Chapter seven consists of the discussion, questioning the validity of the CFD simulations in this thesis. Lastly, in chapter eight, a conclusion is drawn based on the results and discussion.

# 2

# Context

Coastal dunes are of utmost importance for the protection against flooding in many shorelines worldwide. In the Netherlands, this importance is even more significant as large parts of the country lay below sea level (van Bergen & Nijhuis, 2019). As the coastal area is also the most densely populated, the sandy dunes form the first line of defence for most of the Dutch population.

The dunes are not just important for human safety; the Dutch dunes have good conditions for high biodiversity and are home to many plant species and animals. Some endangered species have been reduced to such small amounts that they only occur in the coastal areas (Grootjans et al., 2002). Additionally, large parts of the dunes along the Dutch shore provide clean drinking water (Arens et al., 2013). Lastly, the coastal area is important for tourism, leisure and recreational activities.

## 2.1 Natural dune development

Sand dunes near the coastline are a result of a natural dynamic process of sediment erosion and accretion (Grootjans et al., 2002). This process is maintained by the transportation of sand and dust by the forces of the wind. This movement of sediment by the wind is called aeolian sediment transport (Bagnold, 1941). Aeolian sediment transport can be divided into three modes depending on the size of the sediment particles (Presley & Tatarko, 2009; L. C. van Rijn, 2019):

- **Suspension**: Small particles can lift off due to the wind force and are carried far away
- **Saltation**: Medium size particles bounce across the beach
- **Creep**: Large particles roll and slide across the surface as they are too large to be lifted

Each of these transport modes is visualised in figure 2.1. The majority of wind-driven transport takes place near the ground, up to around a meter above the surface (L. C. van Rijn, 2019).

The aeolian sediment transport is initiated when the wind speed is above a certain threshold. The value of this threshold is dependent on many factors, like the size of the particles and the surface moisture level (Presley & Tatarko, 2009). Sedimentation occurs when the wind speed decreases and the particles are deposited. Sedimentation often happens when the wind speed drops suddenly, and particles are trapped (van Bergen et al., 2021). This happens naturally behind obstacles such as driftwood, shells or vegetation, but man-made obstacles also cause this sedimentation.

## 2.2 Climate change

As mentioned, erosion and accretion are part of the natural dynamic dune development. However, due to a combination of both human and natural activities, there is an increase in dune erosion happening (L. van Rijn, 2011). The natural causes of this decay can largely be attributed to climate change and sea-level rise (de Winter & Ruessink, 2017). de Winter and Ruessink (2017) found a linear relationship between sea-level rise and the

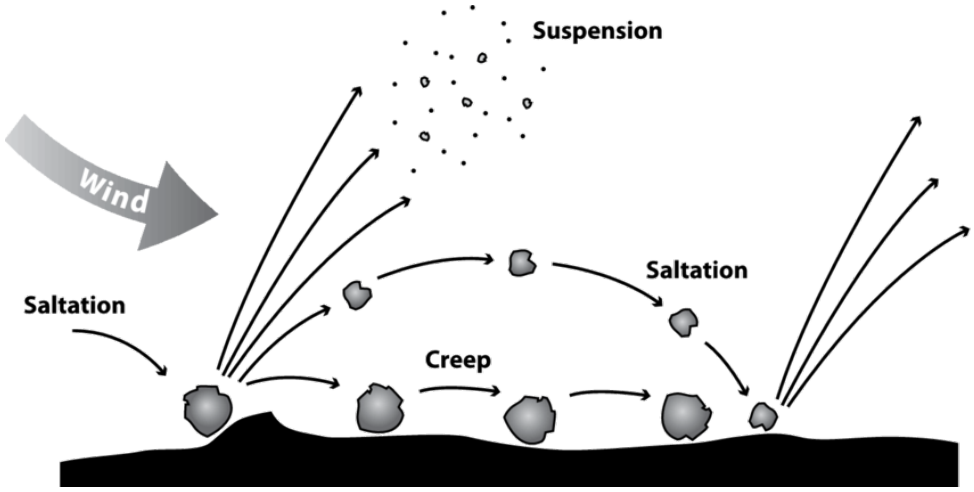


**Figure 2.1.** Three modes of aeolian sediment transport (Presley & Tatarko, 2009)

volume of dune erosion. They suggest this results from an increase in wave height and a growing number of storms that take place as a consequence of climate change.

There are many different predictions about the sea-level rise that we will have to prepare for in the coming decades. In the Netherlands alone, many different climate-change studies are executed. One of the newest studies is done by Deltares (2017), commissioned by the Dutch government. The study presents four different scenarios of the impact of climate change in the coming years. In these four scenarios, the maximum predicted sea-level rise is around 80 cm in 2085. However, more recent studies show that this value might be an underestimation. Haasnoot et al. (2018) estimate that an acceleration in sea level rise might lead to an increased sea level of more than a meter before the year 2100. According to Li et al. (2013), the volume of dune erosion in Noordwijk might increase up to 17 percent, for a sea-level rise of 1.05m in the coming decades.

## 2.3 Artificial dune management

Ever since the 1970s, the Dutch government realised the problem of increased dune erosion and the dangers this might have for the Netherlands (Arens et al., 2013; L. van Rijn, 2011). During that time, the strategy to counteract this erosion consisted of ”hard” measures such as dikes and seawalls (Toimil et al., 2020). This lead to the stabilisation of the foredunes and dunes ridges. These acted as an obstruction, resulting in a drastic limitation of sediment exchange between the beach and dunes. This process is called ”overstabilisation” and can result in a decrease of biodiversity (Arens et al., 2013)

In the 1990’s the interest in this topic increased and awareness grew about the necessity for the improvement of the sea defences in the coming decades because of sea-level rise (Rijkswaterstaat, 1990). After gaining more knowledge about the coastal region, people started to question the use of these hard measures and the long-term effects these might have (Toimil et al., 2020). This led to the first *kustnota*, in which the Dutch government presented a plan for dynamic preservation of the coastline (Rijkswaterstaat, 1990). Since then, artificial sand nourishment operations have been conducted to oppose dune erosion and as a response to sea-level rise (figure 2.2) (Arens et al., 2013). These sand nourishments are considered a ”soft” measure and leave the dunes in a relatively natural and dynamic state (L. van Rijn, 2011). Currently, around 12 million $m^3$ of sand is deposited as nourishments every year (Deltaprogramma, 2012). However, according to (Deltaprogramma, 2020) 20 million $m^3$ is necessary to keep up with the rising sea level.

In some situations, these sand nourishments might not be feasible. For example, if not enough sand is available, or the costs of collecting the sand are unacceptably high. In such cases, ”hard” measures are still used (L. van Rijn, 2011). Alternatively, there are hybrid defence measures, which consists of a combination of hard and soft measures (Toimil et al., 2020).

**Figure 2.2.** Sand nourishments in the Netherlands (Rijkswaterstaat, 2009)

### 2.3.1 Case study: Noordwijk

The dunes of Noordwijk, the location of the case study for this thesis, have such a hybrid measure. The dunes in Noordwijk are reinforced with a dike in 2008 (Arcadis, 2008) as can be seen in figure 2.3. On top of that, there are regular sand nourishments near the Noordwijk coastline. The next nourishment in Noordwijk is planned between 2021 and 2022, consisting of 5.5 million $\mathrm{m}^3$ sand (Rijkswaterstaat, 2021).

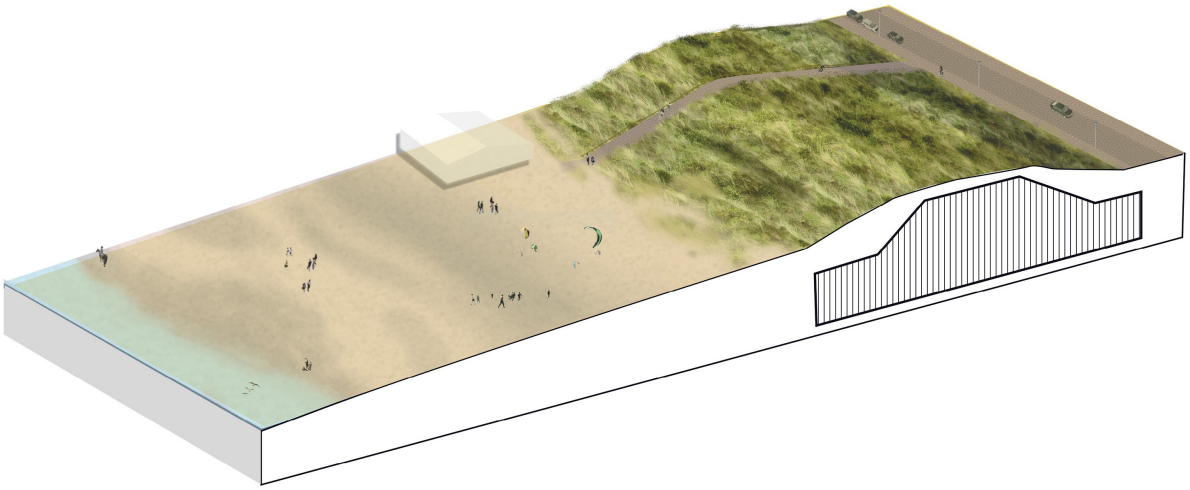

**Figure 2.3.** Dike in dune in Noordwijk (Arcadis, 2008)

## 2.4 Influence of beach buildings on sediment transport

For the sand nourishments to have the desired effect, we count on the aeolian sediment processes to transport the sand towards the dunes. In recent years, beaches have become more and more urbanised (Hoonhout & van Thiel de Vries, 2013). Hoonhout and van Thiel de Vries (2013) conducted a study commissioned by the Dutch Ministry of Infrastructure and Water management to research the influence of beach houses on sediment transport. They analysed readily available data about morphological development, nourishment volumes and beach houses. Their conclusion states that significant morphological changes are happening to the dunes due to man-made structures. Although, it is difficult to determine the magnitude of the problem due to insufficient data.

In 2017 59 different private and public parties agreed on the protection of the Dutch coastline by signing the *kustpact* (Rijkswaterstaat, 2017). This pact aims to preserve the nature, landscape and biodiversity of the coastline and limits the number of buildings allowed on the beaches. In 2019 van Westen (2019) and de Klerk (2019) continue researching the effect of beach housing using photogrammetry and LiDAR data. These studies confirm the conclusions drawn by Hoonhout and van Thiel de Vries (2013). Furthermore, van Westen (2019) says that beach houses can result in static dune characteristics, which harms biodiversity (Arens et al., 2013). van Westen (2019) also stresses the importance to take measures to limit the negative influence of beach houses on sediment transport. Changing the location of the houses towards to dunes, limiting the amount of sand shifting towards the sea and keeping a minimal distance between constructions and beach are suggested as potential measures (van Westen, 2019).

### 2.4.1 Studying the effects of beach houses using CFD

In 2018 van Onselen (2018) was among the first to use CFD modelling to research the effects of different beach house configurations on the sediment transport towards the dunes. To do this, he tested three different measures, (1) placing the houses on poles above the ground, (2) changing the distance from the houses to the dunes and (3) changing the inter-distance between the beach houses. Placing the houses on poles of maximum 1.5 m resulted in the best configuration for unhindered dune ward flow. Combining the poles and inter-distance of around 4 meters between the houses improved the results even more.

This thesis continues with the results from van Onselen (2018) and further studies the effects of different beach house configurations. This thesis proceeds by adding various beach house configurations and taking more varying wind conditions into account.

# 3

# Theoretical Framework

In this chapter the theory behind running CFD simulations in urban environments is discussed. We discuss how to perform important steps before running CFD simulation, such as the creation of the mesh and setting the boundary conditions. Furthermore some best practice guidelines that should be taken into account to ensure reliable results.

Among other things, computational fluid dynamics (CFD) can be used for computer modelling within the field of computational wind engineering (CWE) (Blocken, 2014). As quoted many times, Cermak, 1975 said: ”wind engineering is best described as the rational treatment of interactions between wind in the atmospheric boundary layer and man and his works on the surface of Earth”. In other words, with CFD we can model the interaction between wind and obstacles on the Earth's surface. This could mean natural obstacles such as mountains or trees, but also man-made structures such as buildings. For this research we are mostly interested in using CFD to simulate wind flow around buildings in urban environments.

CFD simulations have multiple advantages over wind tunnel or on-site (scale) measurements for the measurements of urban physics. First of all, it is a way to perform many tests in a structured way in a relatively short amount of time. Furthermore, it allows the user to set the environmental conditions and is therefore not dependent on weather and climate. CFD can also provide detailed information for every part within the computational domain (Blocken, 2014). However, there are also some drawbacks. The accuracy of CFD models is often a point of concern. The results of CFD simulations are highly dependent on the quality of the computational 3D model and the parameters set by the user (Blocken, 2015). For this reason, many guidelines have been set up the help the user obtain reliable results. Examples of some of these guidelines are by Blocken (2015), Tominaga et al. (2008) and Franke et al. (2007).

## 3.1 3D model and computational grid

To generate a CFD simulation for wind flow in an urban environment, we need a 3D model of the buildings we are interested in and the surrounding area. Around this 3D model the computational domain is defined, which is the area where the simulation will be performed. The computational domain needs to be of a certain size to give the flow enough space to flow naturally. The size is dependent on the height $H$ of the highest building within the 3D model (Tominaga et al., 2008) (figure 3.1).

The sides of the computational domain should be at least $5H$ away from the buildings (Franke et al., 2007). The inlet and outlet patch should have a distance of a least $5H$ and $15H$, respectively, to the nearest building (Franke et al., 2007). The z-axis is set at the height of at least six times the height of the highest building within the model (Tominaga et al., 2008).

### 3.1.1 Grid generation

The Navier-Stokes (NS) equations are used to describe the airflow around the 3D model. Since these equations are very complicated, we discretise and simplify the equations to solve them (Eymard et al., 2019; Hirsch, 2007). The most used discretisation method to approximate the wind flow equations is the finite volume

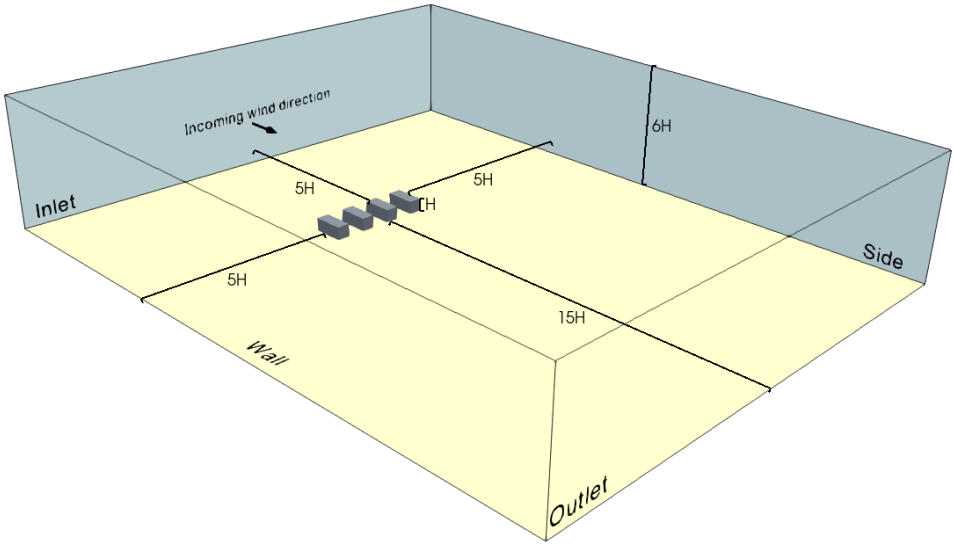


**Figure 3.1.** Minimum size of the computational domain

method (FVM). When using the FVM the computational domain is divided into smaller volumes (Hirsch, 2007). In each of these smaller volumes the flow can be computed (Blazek, 2005).

The subdivision of the computational domain into a detailed mesh is done according to a computational grid (Franke et al., 2007). The creation of the mesh is one of the essential items of running good and accurate CFD simulations (Blocken, 2015; Franke et al., 2007). A good quality mesh makes it easier to reach convergence, is more stable and results in fewer errors. According to Blocken, 2015, the main characteristics of a good quality mesh are the quality of the cells in terms of shape, skewness and a sufficient overall grid resolution.

Generally speaking, the mesh should be fine enough to show important features of the air flow in a satisfactory resolution (Franke et al., 2007; Tu et al., 2018a). According to Tominaga et al. (2008) the minimum grid resolution near buildings should be around $\frac{1}{10}$ of the building scale, in urban environments. Furthermore, it is advised to use at least ten cells in the area between two buildings (Franke et al., 2007). Lastly, according to the best practice guidelines, hexahedral-shaped grid cells are preferred, as these show the least amount of errors (Franke et al., 2007).

### 3.1.2 Law of the wall and y+

Turbulent flow is particularly difficult to model in areas near solid objects, such as the buildings and the ground surface in a 3D model. The air flow in an urban area is affected by the shear stress and turbulence that occur near walls of solid objects (Blocken et al., 2016).

First of all, to model the near-wall-flow accurately it is recommended that the mesh cells near a solid object are parallel to the closest wall of this object(Tominaga et al., 2008). Secondly, to estimate the flow velocity near a wall we use the ”law of the wall”. The (logarithmic) law of the wall estimates the velocity of a turbulent flow at a point close to a solid boundary in the computational domain. The law states that the average velocity of a point in a turbulent flow is relative to the logarithmic distance between this point and a wall (Bradshaw & Huang, 1995; Mandal & Mazumdar, 2015). This law only holds for points near a wall but far enough for the viscous effects to be negligible. Very close to a wall, inside the viscous sub-layer, the viscous effects are high, and the Reynolds shear stress is negligible. Therefore the law does not hold there (Tu et al., 2018b).

To test if the law of the wall can be used to estimate the flow velocity in a model we determine a value $y^+$ for the points closest to the walls within a mesh. $y^+$ is a dimensionless wall unit representing the distance from a point to a wall. The law of the wall is valid for points with $y^+$ value above 30 and up to around 500-1000, this area is known as the ”log-layer” (Blocken et al., 2007; Tu et al., 2018b). If the $y^+$ is below 30, the near-wall point is in the viscous sub-layer or the buffer layer where the law is not valid (Blocken et al., 2007). The near-wall points should be within the scope of the log-layer to accurately predict the flow velocity using the law of the wall.

### 3.1.3 Mesh independence study

Finally, it is necessary to perform a mesh independence study to ensure the mesh is suitable and the uncertainty is as low as possible. Mesh or grid independence means that the results do not change significantly when using a finer mesh, suggesting that the current mesh is refined enough to produce accurate results (Tominaga et al., 2008). The method used to perform the study is based on the method presented by Celik et al. (2008).

For this method, we need three meshes, one fine, one medium and one coarse. Starting with the mesh we plan on using for the simulations as the medium mesh. Then creating the fine mesh by refining the medium mesh with a factor of at least 1.3 and coarsening the medium mesh with a similar factor to make the coarse mesh. We let the simulation run for each of the three meshes until it reaches convergence and extract values of important variables at points of interest. For simulations in urban environments, that would be the wind speed around the buildings and in the wake. Celik et al. (2008) continues by calculating the Grid Convergence Index. For the sake of simplicity and time constraint however, we suggest a simplified method.

By comparing the values of the wind speed from the converged simulations using the three meshes, we can estimate the quality of the results of the medium mesh. If the values of the medium mesh are closer to the values of the fine mesh than they are to the values of the coarse mesh, the quality of the mesh is satisfactory for now.

## 3.2 Flow modelling

The basis for modelling any viscous flow consists of solving the Navier-Stokes (NS) equations (Blazek, 2005). These are a series of differential equations that describe the so-called ”conservation laws” of a fluid. These laws include the conservation of mass, momentum and energy (Blazek, 2005; Hirsch, 2007).

The air flow in urban areas takes place in the lower parts of the atmospheric boundary layer (ABL) (Blocken, 2015). When modelling air flow using CFD we have to take the ABL into account. Flow in the atmospheric boundary layer is turbulent, particularly when close to buildings or other solid objects (Nieuwstadt & Duynkerke, 1996). The turbulence of a flow is measured using the Reynolds number, the higher the number, the more chaos or turbulence a flow has at a certain point.

As mentioned before, to simulate air flow in an urban environment we make use of the Navier-Stokes equations. However, it is very difficult and computationally expensive to calculate the direct solution of the Navier-Stokes equations for turbulent flows (Franke et al., 2007). Therefore there are multiple ways in which the turbulence can be simplified to solve the equations:

- Large eddy simulations (LES): solves only the large-scale turbulent motions (eddies). The smaller scale eddies are filtered out and modeled rather than computed (Blocken et al., 2016). The advantage of LES is that the results give a relatively accurate representation of the turbulence (García-Sánchez et al., 2017). However, for CFD models in urban environments it still requires a large amount of computational effort.
- Reynolds averaged Navier Stokes (RANS): uses only the mean flow to solve the NS equations. All turbulence scales are modelled using a time-averaged value for the Reynold’s number (Blocken et al., 2016). RANS has the major advantage that it is not nearly as computationally demanding is DNS or LES. The drawback is that the turbulence can not be modeled in detail (Blazek, 2005). RANS is most often used in CFD simulations of urban environments (Blocken et al., 2016).

#### Turbulence model

To close the NS equations when using the RANS equations we use a turbulence model to compute the Reynolds stresses (Franke et al., 2007; García-Sánchez et al., 2017). The RANS equations are often used together with a two-equation turbulence model, as this shows generally good accuracy whilst not requiring a lot of computational effort (Blazek, 2005). The standard $k-\varepsilon$ model is one of the most common models used in CFD and showed reasonably good results and stability in previous studies (Franke et al., 2007; Murakami & Mochida, 1989; Pieterse & Harms, 2013; Pourteimouri et al., 2020).

## 3.3 Initial and boundary conditions

Along the sides of the computational domain, there are the inlet, outlet and side boundaries (figure 3.1). The direction of these boundaries change depending on the direction of the incoming flow. For each of the boundaries there are different conditions to take into account.

The conditions for the inlet boundary of a CFD model can be estimated, using calculations to obtain the velocity profile and turbulence characteristics (Blocken, 2015). Using estimates as values for the initial conditions helps the simulation converge and reduces computation time. The most commonly used formulae for RANS CFD simulations using the standard $k-\varepsilon$ turbulence model are the ones presented by Richards and Hoxey (1993) shown in equations 3.1, 3.2 and 3.3 (Blocken, 2015).

$$U(z) = \frac{u_*}{\kappa} \ln\left(\frac{z + z_0}{z_0}\right) \tag{3.1}$$

Equation 3.1 gives the wind speed $U(z)$ at elevation $z$ using the shear velocity $u_*$. $\kappa$ is the von Karman's constant, set at 0.42. $z_0$ is the aerodynamic roughness length of the ground surface. The value for $z_0$ in meters depends on the type of terrain. Open smooth terrain such as beaches or deserts have a low $z_0$ value of around 0.005 m (Blocken, 2015). In very rough terrain such as forests or city centers $z_0$ can go up to more than 2 m (Blocken, 2015).

$$k = \frac{u_*^2}{\sqrt{C_\mu}} \tag{3.2}$$

$$\varepsilon = \frac{u_*^3}{\kappa(z + z_0)} \tag{3.3}$$

Richards and Hoxey, 1993 also present equations for the inlet turbulent kinetic energy $k$ (equation 3.2) and the turbulence dissipation rate $\varepsilon$ (equation3.3). In equation 3.2$C_\mu$ is a constant equal to 0.09.

These equations assume constant shear stress with height, which only holds in the lower parts of the atmospheric boundary layer (Tominaga et al., 2008). It is necessary to check that the height of the computational domain is within the lower parts of the atmospheric boundary layer. According to Blocken et al., 2007, this is around 200 m high in open terrain such as a beach, but the height can be much higher above an urbanised area.

The wall boundary conditions are used for solid items in the computational domain (Tu et al., 2018b). In urban environments this means the ground surface, the buildings and vegetative obstacles such as trees. Each of these items has its own characteristics and, therefore, different boundary settings.

## 3.4 Aeolian transport model

The potential sediment transport on a beach is dependent on many factors, such as wind direction, speed, moisture levels, particle size and fetch distance (Delgado-Fernandez, 2011). In this thesis however we assume the particle size and moisture levels to be constant throughout the simulations, and the fetch distance to be long enough to let the flow develop fully (Delgado-Fernandez, 2011). For the calculations of sediment transport we only take variations in wind direction and wind speed into account. Using the extracted points with wind speed values, we can estimate the sediment transport that could occur at a certain point. Bagnold, 1937 was the first to create an analytical aeolian transport model based on physics and incorporated the boundary layer theory (Sherman & Li, 2012). His model, given at equation 3.4, is still widely used and produces reasonably good results, similar to other, more recently created, models (Sherman & Li, 2012; Sherman et al., 2013).

$$q = C_B \left(\frac{\rho_a}{g}\right) u_*^3 \left(\frac{d}{D}\right)^{\frac{1}{2}} \tag{3.4}$$

Bagnolds model calculates the transport rate $q$ in $kgm^{-1}s^{-1}$, using the density of the air ($\rho_a$), the shear velocity ($u_*$) and the median grain size ($d$). $C_B$ is a constant set 1.8 for sand grains that are similar in size (Bagnold, 1941). D is a reference grain diameter, for which the value 0.25mm is typically used (Bagnold, 1941). g is the gravitational acceleration, 9.81 m/s.

Before determining the transport rate, we set a threshold flow velocity ($U_t$), the wind speed. We start with calculating the threshold shear velocity, using equation 3.1.

$$u_{*t} = A\left(\frac{\rho_s - \rho_a}{\rho_a} g d\right)^{1/2} \tag{3.5}$$

In equation 3.5 $u_{*t}$ is the threshold shear velocity. This is calculated by taking the air density ($\rho_a$) and surface density of the sand ($\rho_s$). A is a constant set at 0.1 (Bagnold, 1941). The value of the shear velocity is only valid for points close to a wall, for example the ground surface (section 3.1.2). To determine the threshold flow velocity ($U_t$) for a point further away from the surface, we use the law of the wall, in equation 3.1. The threshold flow velocity can be calculated by inserting the result of equation 3.5 together with the height $z$ of the point into equation 3.1. If the wind speed in a cell is below the threshold velocity, we refrain from any further calculations on the cell and assume no sediment transport take place.

Equation 3.4 shows the transport in any direction, and we are primarily interested in the dune-ward direction of transport. Therefore we suggest combining equation 3.4 with the model proposed by Davidson-Arnott and Law (1996) in equation 3.6.

$$Q_D = 0.1q\cos(\alpha) \tag{3.6}$$

Equation 3.6 calculates the dune-wards sediment transport, using $\alpha$ as the angle between the approaching wind direction and the shore perpendicular. Delgado-Fernandez, 2011 uses this method and specify it further by determining conditions that should be satisfied for the potential of dune-ward sediment transport. As we do not take moisture levels into account, we only use the conditions relevant to our model. The relevant conditions regarding the wind speed $U$ are:

- $U > U_t$, the wind speed should be higher than the threshold flow velocity
- $U$ should have an onshore component. This means that we look at the three individual components of the vector $U$, as $U_x$, $U_y$ and $U_z$. The component in the x-direction, perpendicular to the shore, should have a positive value, meaning it is going towards the dunes.

In all cells that fulfil both these conditions, $q$ and $Q_D$ can be calculated.

# 4

# CFD Methodology

This chapter explains the methodology used to run CFD simulations and defines the parameters to create different scenarios. The process of running one simulation consists of roughly four parts: the creation of the 3D models, the creation of the mesh, the setting and running of a simulation itself and the post-processing. The last sections of this chapter explain the parameter variations used for running the simulations. It starts with the variations between different beach house configurations and moves on with different values used for the incoming wind flow.

## 4.1 Pre-processing

### 4.1.1 Creation of 3D models

The 3D models used for running the simulations consist of three elements; two digital terrain models (DTMs), one of the beach and one of the dunes. The third element consists of the beach houses themselves. This way, all three parts can be given different characteristics, such as roughness factors, when running the simulations. The beach and dunes are modelled based on a section of Noordwijk beach (van Bergen et al., 2021), from the sea till the boulevard, with a total length of 240 m. The houses length, width and height, are 7 x 3 x 3 meter, respectively.

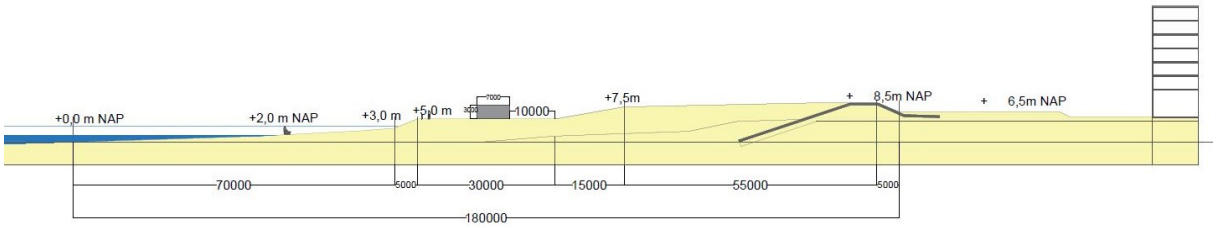


**Figure 4.1.** Section Noordwijk (van Bergen et al., 2021)

The terrain models of the beach and the dunes are modelled using Grasshopper 3D, a visual programming language within the Rhinoceros 3D CAD application. Grasshopper allows the use of a parametric modelling approach, making it easy to change the models during the research process. The created DTMs can be exported as Standard Triangle Language (STL) files. The full grasshopper model is visualised in appendix B.1.

The 3D model of the beach houses is made using a Python script (section 5.2). The Python codes take a STL file of one single building and edit this into a configuration based on pre-defined parameters. Different configurations of the beach houses are made by changing one parameter at a time. Whilst running the simulations, we would like to automatically change the beach houses' configuration, as this would allow us to run many configurations in a row. By doing the parameterisation in Python, new configurations can be created in a systematic step-wise matter. Lastly, the houses, the beach and the dunes models are then merged into one model.

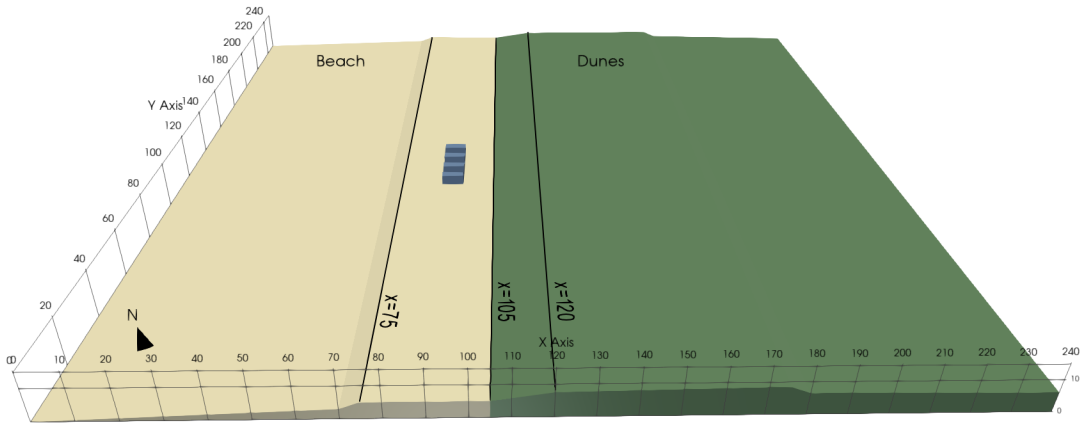


**Figure 4.2.** Example of one of the 3D models

### 4.1.2 Creating the mesh

Around the 3D model, the computational domain is defined, which is where the simulation will be performed. The computational domain is then split into a grid of many small volumes to approximate the airflow using the FVM. The grid is created using the tool cfMesh. cfMesh is an open-source library for the creation of CFD meshes separate from OpenFOAM (CfMesh, 2021).

The basis of the mesh is done by creating a Cartesian mesh, which uses hexahedra primarily, according to the best practice guidelines (Franke et al., 2007). cfMesh also allows the addition of refinement areas, which allows creating a fine mesh around the area of interest, the beach houses and the wake of the houses, whilst leaving the mesh coarse far away from the houses (figure 4.3). In order to minimise the error of the results near wall boundaries in the model, there is an added option to add boundary layers parallel to the boundary and refine the mesh even more (Tominaga et al., 2008; Tu et al., 2018a).

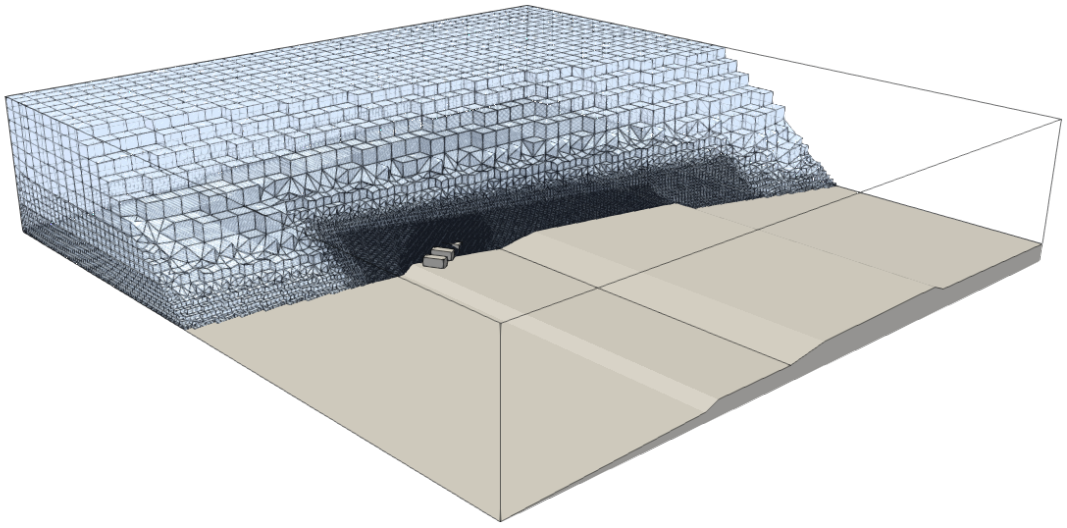

**Figure 4.3.** Mesh created using cfMesh

#### y+ values of the mesh

We calculated the $y^+$ for all the points within the computational domain to test the mesh. In section 3.1.2 it is described that the values of $y^+$ must be above 30 and have a maximum value of around 1000. As shown in figure 4.4 the $y^+$ values near the beach houses and around the wake are much lower than further away in the mesh. This difference is because the mesh is a lot more refined in those areas; therefore, the distance from a point to the surface will be much smaller.

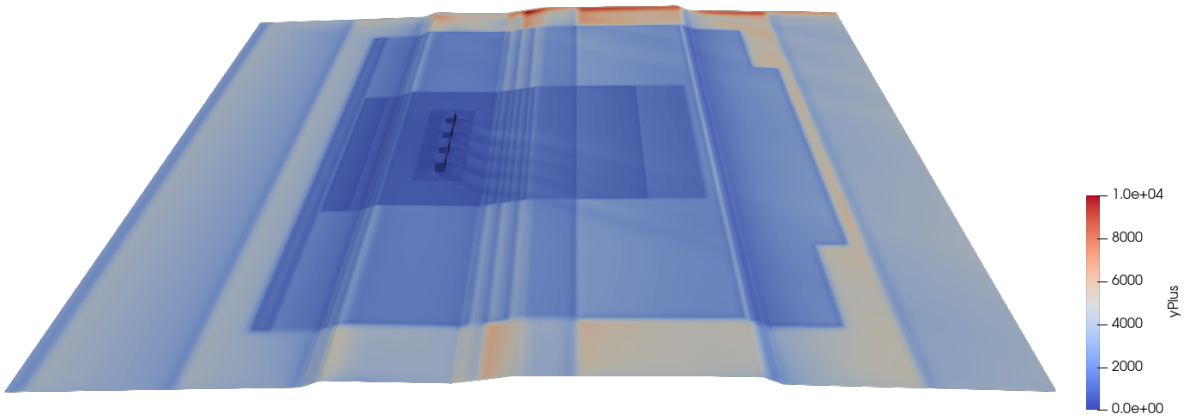


**Figure 4.4.** y+ values around mesh

Table 4.1 shows the minimum, maximum and average values for the mesh shown in figure 4.4. Since we are mostly interested in the area around the buildings, the beach and dunes patch values are not as relevant. The values from the buildings range from 60 to around 1000 and average around 420. These values are well within the minimum boundary of 30. Therefore we can conclude that the quality of the mesh is satisfactory to model near-wall flows.

**Table 4.1.** y+ values for a mesh at time of convergence

| # Time | patch | min | max | average |
|---|---|---|---|---|
| **865** | beach | 65.13 | 6880.09 | 1164.13 |
| **865** | buildings | 60.80 | 1088.96 | 420.80 |
| **865** | dunes | 465.69 | 10205.7 | 1919.33 |

### Mesh independence

Furthermore, as mentioned in section 3.1.3, we need to ensure that the mesh is detailed enough to give reliable results. To do this, we perform a mesh independence study as suggested in section 3.1.3. Starting with three meshes, the mesh we plan on using as the medium mesh, a coarser mesh and a finer mesh. We then let simulations run on all three meshes and compared the results. In all three meshes, we sampled the wind speed at nine points, divided over three lines, one at x=75 m, one at x=105 m and one at x=120 m (figure 4.2). By comparing the meshes' values, we determined if the fine mesh results or coarse mesh results are closer to the medium mesh.

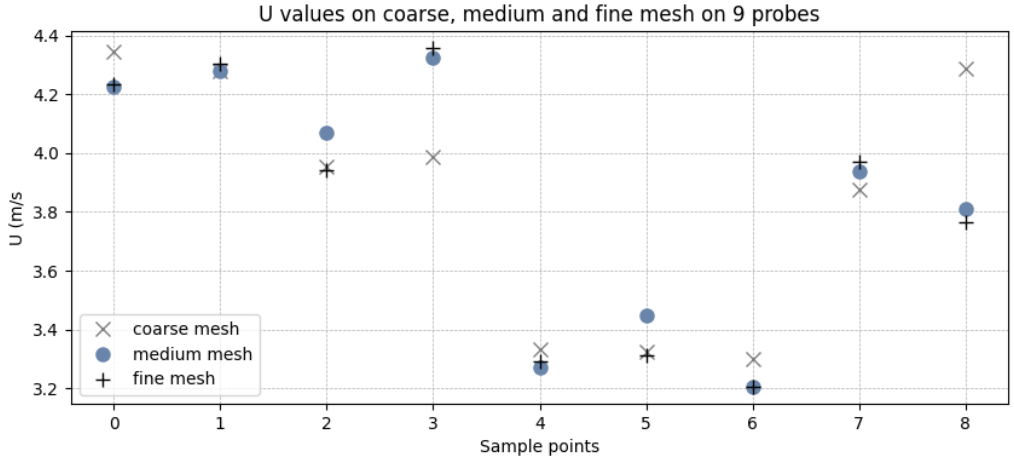


**Figure 4.5.** Values of nine probes compared with three meshes

One way of doing this is by calculating the difference between the coarse mesh values and medium mesh values as $\varepsilon_{12}$, and the difference between the fine mesh and medium mesh values as $\varepsilon_{32}$. Table 4.2 shows the difference of the sample points between the three meshes, averaged along each x-line. $\varepsilon_{32}$ is lower on all three lines, suggesting that the results of the medium mesh are indeed closer to the fine mesh than they are to the coarse mesh.

**Table 4.2.** Difference between the results of the mesh to a finer mesh ($\varepsilon_{32}$) and to a coarser mesh ($\varepsilon_{12}$). The results are averaged from sample points along three lines.

| Line | $\varepsilon_{12}$ (m/s) | $\varepsilon_{32}$ (m/s) |
|---|---|---|
| **x = 75 m** | 0.080 | 0.055 |
| **x = 105 m** | 0.174 | 0.065 |
| **x = 120 m** | 0.211 | 0.026 |

## 4.2 Simulations

The computational fluid dynamics (CFD) simulations are performed using OpenFOAM (v8), an open-source CFD toolbox (OpenCFD Ltd., 2016). OpenFOAM solves the Navier-Stokes equations using a certain solver that can be determined by the user, depending on a type of flow. It returns values of multiple attributes, dependent on the solver, for each cell within the computational domain. Additionally, it also allows doing some post-processing on the results.

### 4.2.1 Solver set-up

For the simulations in this thesis, we used the solver called "SimpleFoam". This is a solver for steady-state, incompressible turbulent flow using the FVM (section 3.1.1). The solver calculates the wind speed (U), pressure (p), turbulent viscosity (nut), turbulent kinetic energy (k) and turbulent kinetic energy dissipation rate ($\varepsilon$) for any point within the 3D mesh of the computational domain. To simplify and approximate the Navier-Stokes equations of the wind flow the RANS equations are used (section 3.1.1). The RANS equations are used together with the standard two-equation $k-\varepsilon$ turbulence model, which is necessary in order to close the equations (Blazek, 2005).

### 4.2.2 Boundary conditions

Before running the solver, we need to ensure the boundary conditions fit the scenario in question. Along the sides of the computational domain, there are the inlet, outlet and side boundaries (figure 3.1). The boundaries change depending on the direction of the incoming flow. Furthermore, we need to take the ABL into account when selecting the boundary conditions.

To set up the initial conditions of the inlet boundary, we use the formulas as presented by Richards and Hoxey (1993). We are using equation 3.1 to determine the shear velocity $u_*$ by inserting the speed of the incoming wind $U(z)$ at 10 m height ($z$) and the aerodynamic roughness length $z_0$ of the ground surface. On the beach $z_0$ has a value of 0.005 m, for open and smooth terrain (Blocken, 2015). In the dunes, where there is vegetation, we use a roughness length of 0.03 m, the value for open landscape with low vegetation (Blocken, 2015). The value of $z_0$ for the inlet boundary depends on the direction of the wind.

**Table 4.3.** Boundary settings in OpenFOAM

| | $U$ (m/s) | $p$ ($m^2/s^2$) | $k$ ($m^2/s^2$) | $\varepsilon$ ($m^2/s^3$) | $nut$ ($m^2/s$) | $z_0$ (m) |
|---|---|---|---|---|---|---|
| **Inlet** | atmBoundaryLayerInletVelocity | zeroGradient | atmBoundaryLayerInletK | atmBoundaryLayerInletEpsilon | calculated, 0 | - |
| **Outlet** | inletOutlet | totalPressure | inletOutlet | inletOutlet | calculated, 0 | - |
| **Side** | slip | slip | slip | slip | calculated, 0 | - |
| **Beach** | noSlip | zeroGradient | kqRWallFunction | epsilonz0WallFunction | nutkAtmRoughWallFunction | 0.005 |
| **Dunes** | noSlip | zeroGradient | kqRWallFunction | epsilonz0WallFunction | nutkAtmRoughWallFunction | 0.03 |
| **Buildings** | noSlip | zeroGradient | kqRWallFunction | epsilonWallFunction | nutkWallFunction | - |

The wall boundary conditions are used for solid items in the computational domain (Tu et al., 2018b). In this thesis, this means the beach, the dunes and the buildings fall under this category. Each has its own

characteristics and, therefore, different boundary settings. The beach and dunes are ”rough” walls that influence the velocity of the air flowing near it. For this reason, we set the aerodynamic roughness length for the boundary conditions of these walls. The final boundary settings used in OpenFOAM are shown in table 4.3.

### 4.2.3 Running the solver

With all the settings for the scenario saved correctly, we can start running the actual simulation using the solver. The simpleFoam solver runs iterations until it reaches convergence, which is estimated to be at the time the residuals are below a certain threshold (Franke et al., 2007). The threshold for all residuals are set at 1e-4 (figure 4.7). Secondly, we plot the values of several points, called probes, during the simulation run. To check if the solver has reached convergence, the values of the probes should have stabilised (figure 4.6). In this case, we tested the wind speed at nine probes at different locations since wind speed is the value in which we are interested.

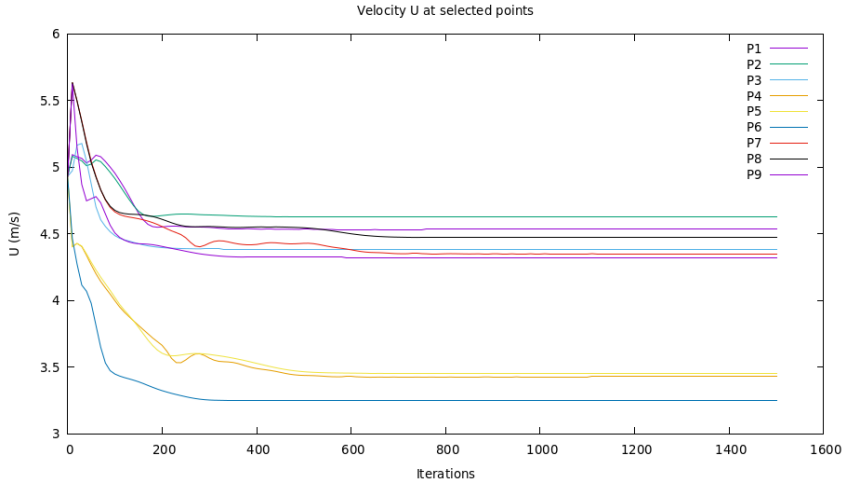


**Figure 4.6.** Probes: wind-speed in 9 points until convergence

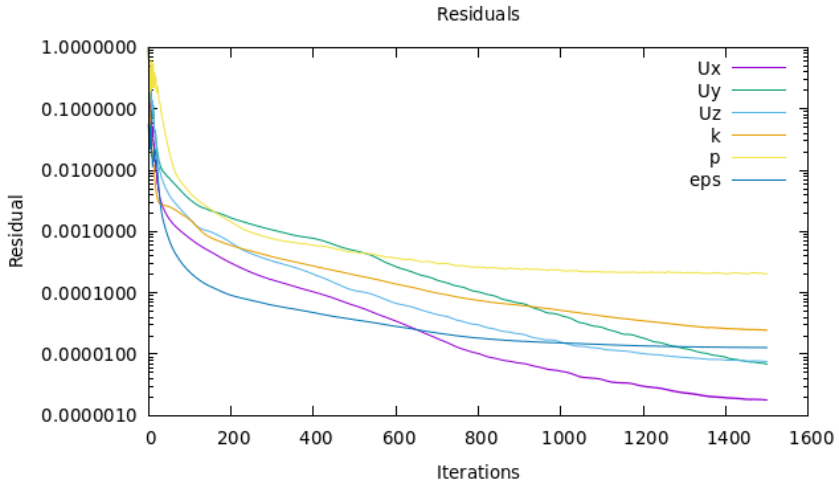


**Figure 4.7.** Residuals of iterations until convergence

The user can also specify the end time at which iteration the solver should stop regardless if it has converged or not, as well as the time step in which the output should be written to a file. The solver calculates the parameters mentioned in section 4.2.1 for all cells within the computational domain. The results are stored during every written timestep and contain the parameter values for every cell in the computational domain.

## 4.3 Post-processing

Once the solver has finished, the results can be visualised and processed in the post-processing tool ParaView. For this thesis, we are interested in the wind speed, particularly close to the surface, as that is where the sediment transport mostly occurs. To limit the amount of data, a cutting plane is extracted from the wind speed at the time of convergence. This plane is extracted at $\frac{1}{10}$ of the building height, 0.3 m, above the surface, following the beach and dunes profile. The extracted plane consists of a 0.2x0.2m grid of points (figure 4.8).

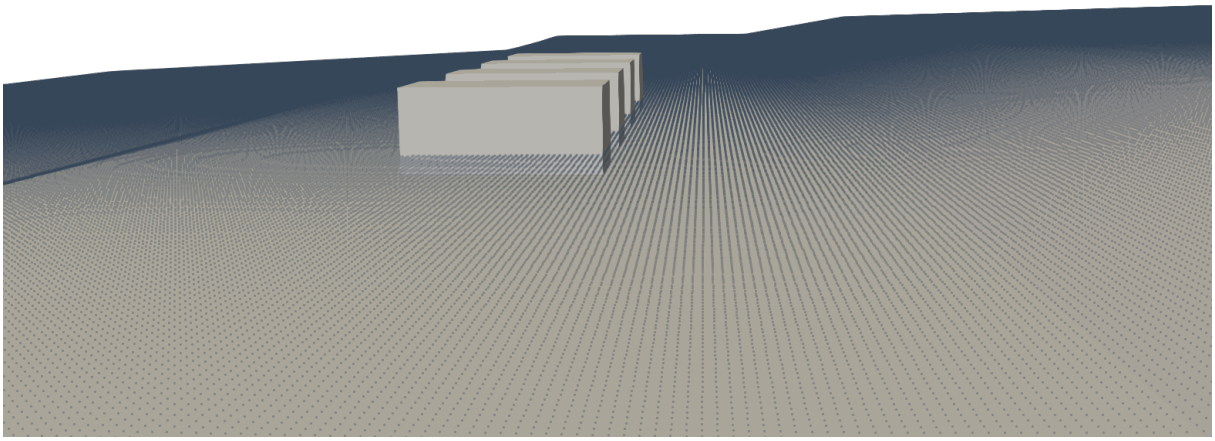

**Figure 4.8.** Extraction of points at 0.5m above surface

### 4.3.1 Dune-ward sediment transport

The extracted plane is used to calculate the dune-ward sediment transport. Using the wind speed and direction for all points within the plane we use the formula suggested by Bagnold (1941) (equation 3.4) to calculate the total sediment transport that takes place. Additionally using the method suggested by Delgado-Fernandez and Davidson-Arnott (2011) (equation 3.6) we can determine the amount of sediment transport moving in the direction of the dunes.

### 4.3.2 Conversion to a georeferenced raster

The created VTK files from the extracted plane are transformed to a raster file to georeference them. By eliminating the z-value from the 3D file, every point's x and y values can be stored in a 2D tiff file.

The tiff file is then translated using the x and y value of a point in Noordwijk using the Amersfoort / RD New coordinate reference system (CRS). The coordinates of the transformation are based on the location of the actual beach houses in Noordwijk that were observed during a site visit (appendix A. Since orientation of the Dutch shore goes from SW to NE, the raster is rotated as well. This leads the following transformation matrix:

$$A = \begin{bmatrix} -0.5 & 0.87 & 90025.4 \\ -0.87 & -0.5 & 474520.2 \\ 0.0 & 0.0 & 1.0 \end{bmatrix}$$

Applying the transformation matrix to the tiff file and visualising this in QGIS gives the result as shown in figure 4.9.

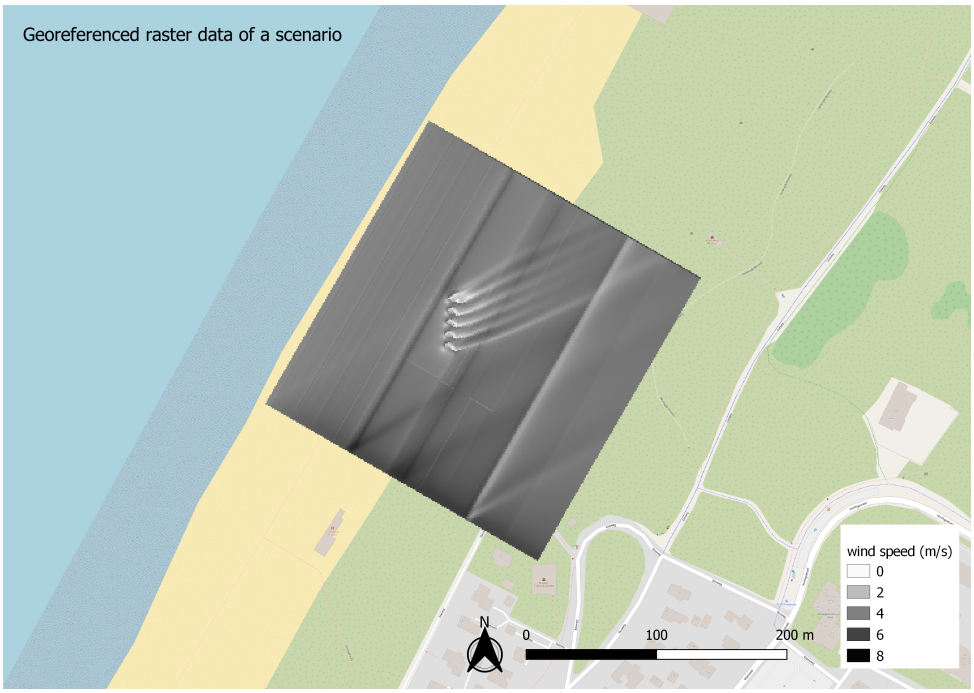


**Figure 4.9.** Georeferenced raster data of a scenario in Noordwijk

## 4.4 Parameter variation

### 4.4.1 Beach house configurations

By creating different beach house configurations, we can observe what configuration has the best effect on sediment transport. The configurations that are tested are based on previous results by van Onselen, 2018 and suggestions from ShoreScape (van Bergen et al., 2021). van Onselen (2018) tested the effects of changing the height of the houses, the distance between the houses and the sea and the distance between the houses themselves. He found that putting the houses on 1.5 m poles had the desired effect of blocking the sediment transport as little as possible. Changing the distance towards the dunes had negligible effects. ShoreScape suggested that minimising the wind facing surface would limit the sediment transport the least based on scale models. We use this as a starting point by rotating the houses so that they face the prevailing wind direction.

#### Configuration group 1

We started by simulating the effects of changing the angle of a whole row of five beach houses compared to the shore. The first simulation starts parallel to the shore, similar to the way the beach houses are often placed (appendix A). The distance between the houses is 4 meters, based on the recommendations of Hoonhout and van Thiel de Vries (2013). They advise that the distance between the houses should be at least as much as the width of the houses themselves. The distance from the dune foot is initially 15 meters, but this changes as the houses rotate. The angle between the shore and row of houses increases from 0 degrees by steps of 20 degrees until it reaches 60 degrees (figure 4.10).

#### Configuration group 2

Following this first group of simulations, we continued with a second group by changing the angle of each beach house individually (figure 4.11). We are starting with the houses facing the sea and changing the angle of each house with an increment of 30 degrees until the house is parallel to the shore (90 degrees).

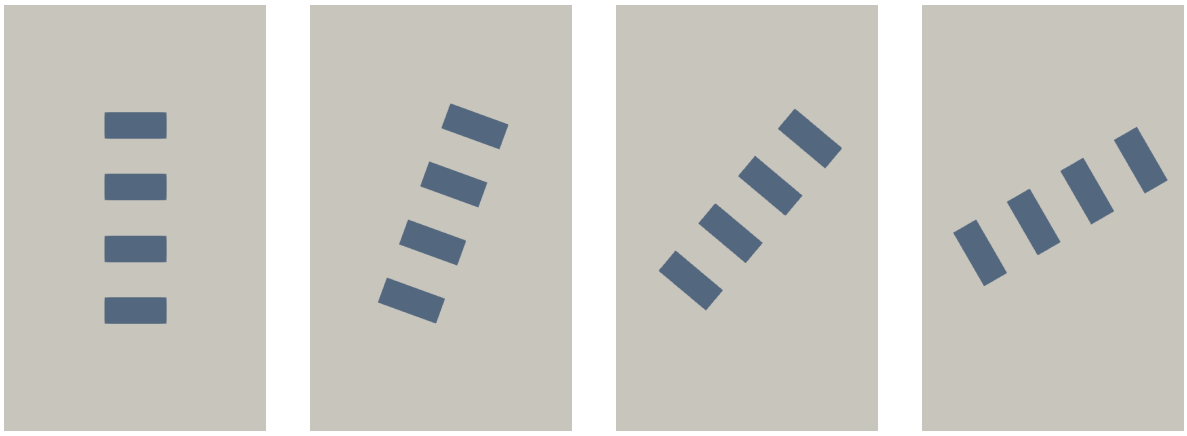

(a) 0 degrees (b) 20 degrees (c) 40 degrees (d) 60 degrees

**Figure 4.10.** Configurations group 1: changing the angle of the row of beach houses

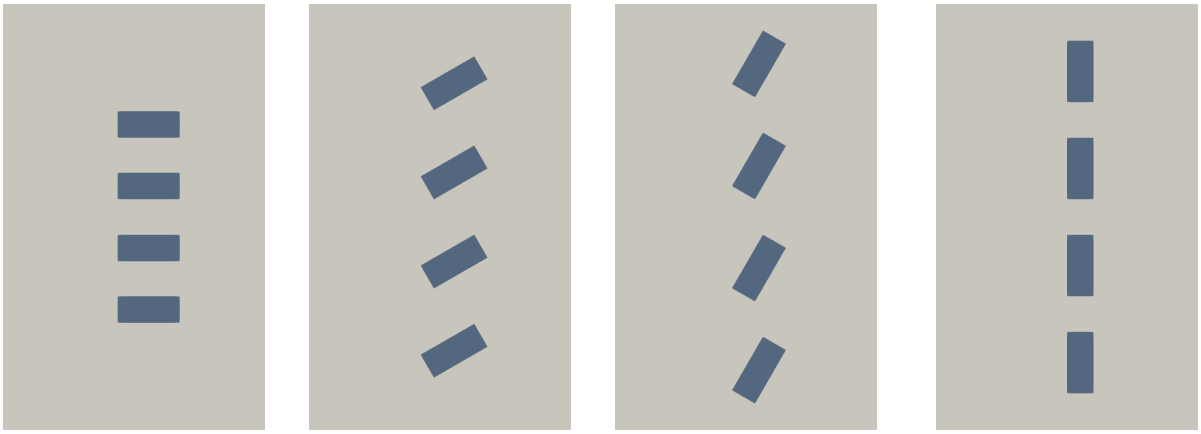

(a) 0 degrees (b) 30 degrees (c) 60 degrees (d) 90 degrees

**Figure 4.11.** Configurations group 2: changing the angle of every beach house individually

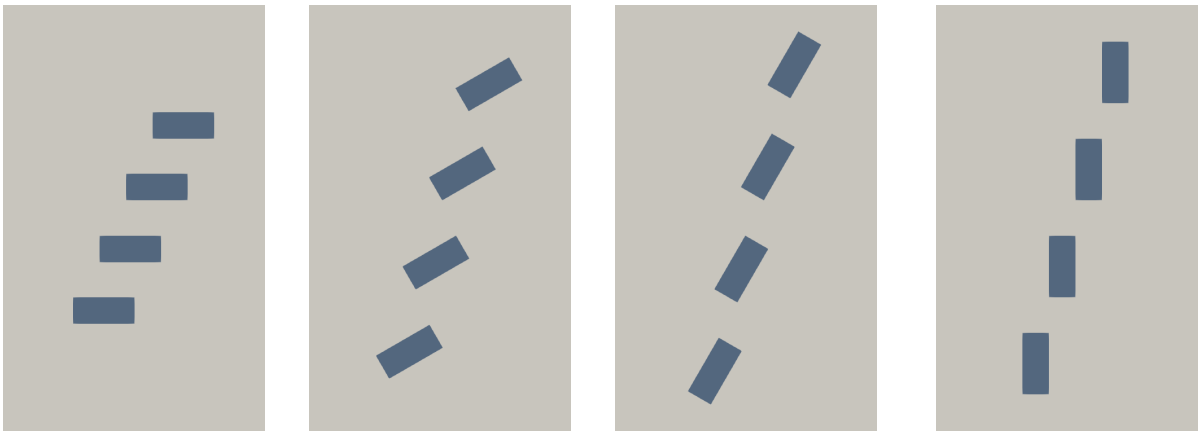

(a) 0 degrees (b) 30 degrees (c) 60 degrees (d) 90 degrees

**Figure 4.12.** Configurations group 3: changing the individual angle and the row angle of the beach houses

### Configuration group 3

After initial analysis of the results of group 1 and 2 and seeing the potential of these configurations, we wanted to simulate a combination of these two previous groups. We do this by placing a row of the houses under a slight angle, similar to the 20 degrees angle from configuration group 1. This way, we minimise the surface facing the prevailing wind direction. The houses are then also rotated individually, again from facing the sea to parallel to the shore (figure 4.12).

### Configuration groups 4 and 5

The next two groups of configurations are based on suggestions from ShoreScape. Group 4 consists of placing the houses in stair-like shapes. Group 5 places the houses in a v-shape. The hypotheses are that a v-shape would act as a funnel and increase wind speed. As a consequence, this might lead to an increase in sediment transport. In order to show these two groups, we need at least six houses. This means the results from these groups will not be comparable to the other groups straight away. Figure 4.13 and 4.14 show the configurations.

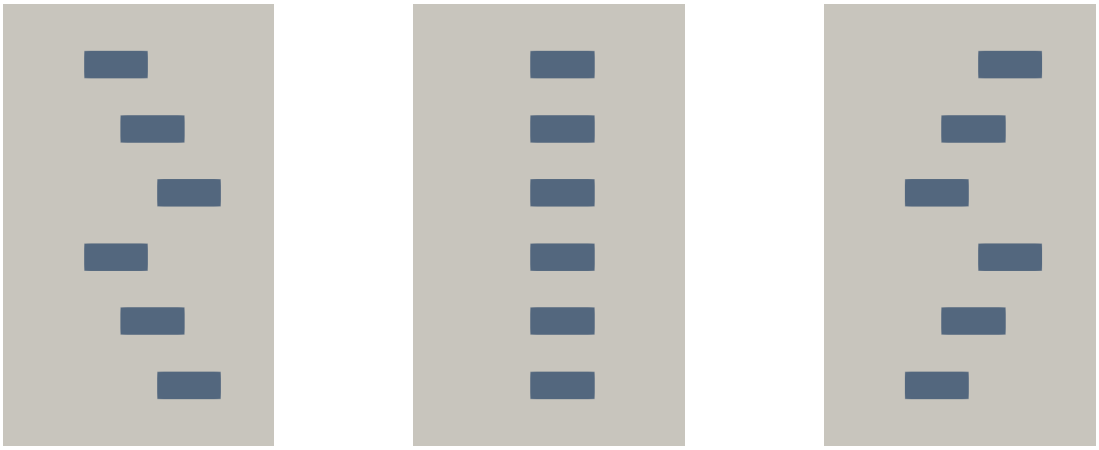

(a) Stair-shape first direction (b) straight line, for comparison (c) Stair shape second direction

**Figure 4.13.** Configurations group 4: stair shapes

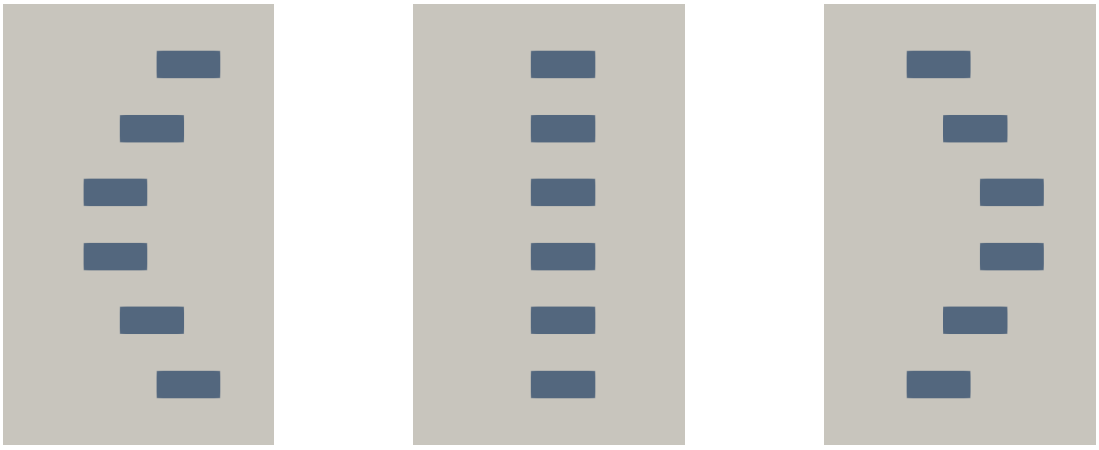

(a) v-shape pointing towards sea (b) straight line, for comparison (c) v-shape pointing towards dunes

**Figure 4.14.** Configurations group 5: creating v-shapes

### 4.4.2 Wind parameters

For this thesis, we based the model on a section of the beach of Noordwijk. Therefore it would be the most accurate to use wind data from Noordwijk as well. The Dutch Meteorological Institute publishes their data on an open data platform (KNMI, 2021). One of these data sets contains modelled wind data for every hour from 2014 to august 2019. The data is available for 10-200 meters above sea level for every location in the Netherlands using a 2.5 km grid size (KNMI, 2019). Since the beach houses are only on the beach from April till October, we selected only those values. Furthermore are we only interested in the wind at 10 meters height, since these are the closest to the buildings.

Figure 4.15 shows the distribution (in percentage) of wind directions from April to October in Noordwijk averaged over the years 2014 to 2019. The WSW direction is the most prevalent, which is similar to the most prevalent wind in the whole of the Netherlands. Figure 4.16 shows the average wind speed for all the before mentioned directions. The wind coming from the WSW is not only the most prevalent but also has the highest wind speed. It is important to note that these figures are based on modelled data, not actual measurements.

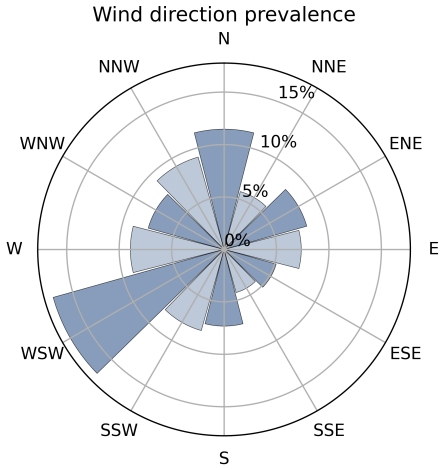


**Figure 4.15.** Wind direction distribution in Noordwijk from April till October (KNMI, 2019)

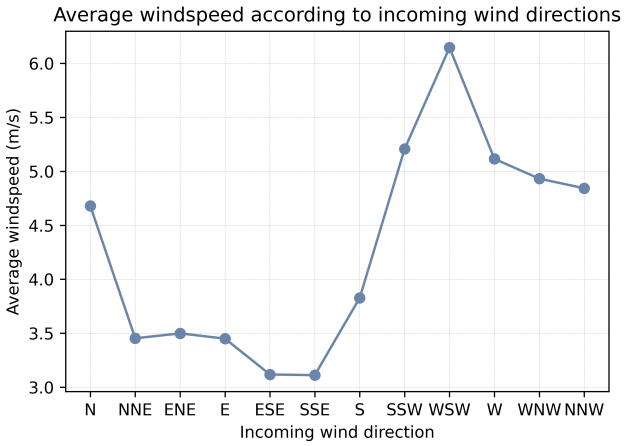


**Figure 4.16.** Average wind speed per wind direction in Noordwijk from April till October (KNMI, 2019)

To accurately represent how the beach houses influence sediment transport, we should take all wind directions into account. Therefore every configuration is simulated twelve times, once for every wind direction. For every wind direction, the average wind speed is used as the initial value for the OpenFOAM simulation. This means the boundary conditions also change for every simulation (section 3.3). Weighing the results from the simulations then according to their occurrence (table 4.4) gives a seasonal estimate of the (dune-ward) sediment transport.

**Table 4.4.** Occurrence and avg wind speed for every wind direction

| Wind direction | N | NNE | ENE | E | ESE | SSE | S | SSW | WSW | W | WNW | NNW |
|---|---|---|---|---|---|---|---|---|---|---|---|---|
| **Occurrence** | 0.115 | 0.057 | 0.082 | 0.074 | 0.052 | 0.043 | 0.073 | 0.080 | 0.169 | 0.089 | 0.075 | 0.091 |
| **Avg. wind speed (m/s)** | 4.680 | 3.453 | 3.499 | 3.450 | 3.118 | 3.112 | 3.828 | 5.207 | 6.146 | 5.115 | 4.932 | 4.843 |

#### Wind facing surface

Upon suggestion from Shorescape, we want to examine the connection between the wind facing surface of a configuration and sediment transport. With the wind facing surface, we mean the area of the houses that can be seen when looking towards the direction in which the incoming wind flows. This means that the wind facing surface changes depending on the direction of the wind. The hypotheses behind the wind facing surface are that the smaller the surface facing the wind, the less wind is blocked and the less sediment transport is affected.

# 5

# Database storage and automation

In the previous chapter, we discussed running CFD simulations and creating different scenarios by varying the configurations and wind conditions. Since there are many simulations to run and all need different parameters and OpenFOAM settings, it would be much effort to do this manually, especially while keeping up with a large amount of data and results generated. We use a database where all necessary information and settings for all scenarios are stored to automate the process. A series of Python scripts can link the database with OpenFOAM and run the simulations using the settings as provided within the database. After running the simulations, including the analysis and post-processing, the results are stored back in the database. This enables us to compare the results from the scenarios easily.

The main advantage of using a database is to store a large amount of data in an organised way. Within this thesis, it is also of added value to quickly compare the results for the different wind directions and scenarios. Furthermore, the database makes it possible to keep track of the results while running the simulations, as it can store simulations metadata. For example, the timestamps at which the solver starts running and finishes tells the user how long every simulation took. Lastly, database storage is an easy way to share the results and findings when working with others.

## 5.1 Set up of the database

To store the simulation settings and resulting data, we implemented a PostgreSQL database. PostgreSQL is an open-source database management system (DBMS) using, as the name suggests, Structured Query Language (SQL) for queries. PostgreSQL has a geospatial data add-on named PostGIS. PostGIS allows the possibility to store geographical information system (GIS) data such as georeferenced raster files in the database.

#### Related work

Although some similar implementations of DBMS has been done by others (Chakrabarty & Shih, 2004; Dillavou et al., 2008; Yu et al., 2012) information about the storage of CFD data in a database system is very limited. Yu et al., 2012 present a method to handle data from numerical models, such as CFD models, in a GIS-based DBMS. They store all resulting data within the database, including geospatial data using PostGIS. Similarly Dillavou et al., 2008 uses a database to store CFD specific data. However, they minimise the load on the database by not storing large amounts of data directly but by only linking to it and keeping track this way.

#### Development process

As there is no standardised way of storing CFD data in a DBMS, we set up our own data model from scratch. The development of a database we used consists of four parts (figure 5.1). We are starting with a requirement analysis to consider what we need from our database and its function. This is then translated into a UML class diagram to show what data classes we need and how the classes are connected. The UML diagram acts as an initial model for the design of the database in PostgreSQL. The last part consists of the implementation, where we use the database to store, retrieve and compare CFD data.

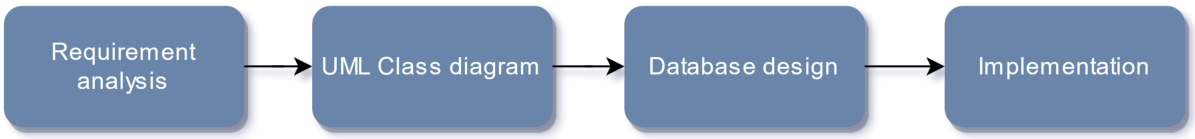


**Figure 5.1.** Database development process

### 5.1.1 Data requirement analysis

The process started with considering all required data and parameters necessary to run one simulation in OpenFOAM and perform the post-processing afterwards. The requirements are grouped according to the chronological order in which someone needs the parameters when running CFD simulations.

There are certain *general parameters* that are necessary to determine before running any OpenFOAM simulation. Those are settings such as what solver to use and what timestamp to use as the end time (section 4.2.1). Furthermore, we need the variables for several *environmental parameters*, such as the air density and the aerodynamic roughness length of the ground surface, to run the simulations and to perform the post-processing. These general and environmental parameters will not be changed during the simulations but must be set by the user before starting.

#### Configurations and mesh

First, we need to have a 3D model of the beach, dune and the *configuration* of beach houses on top of this. To generate a particular model, we need to know several *configuration parameters*, such as the number of beach houses, the x-y coordinates of these houses and the distance between them. If we want to run simulations on a *group of configurations* in sequence, we need to store the parameters for all these configurations. Furthermore, when generating the computational domain and the mesh, OpenFOAM needs to know which 3D file to use and where this is stored.

#### Scenarios and Flow parameters

As mentioned in section 4.4.2 every configuration is used for at least twelve simulations, one for every wind direction used. All these twelve simulations together form a *group of scenarios*, multiple groups can be linked to one configuration if you would want to change parameters between groups. Each of these simulations using a specific wind direction and parameters is what we call a "*scenario*".

For every scenario, we need to set the *flow parameters*, such as the direction and speed of the incoming wind. The wind speed is set to the wind average speed that belongs to the direction according to the KNMI *wind data* (section 4.4.2). Additionally, depending on the wind conditions, we define the boundaries and initial conditions. All *four boundaries* of the computational domain have to be assigned to either the inlet, the outlet or the side boundary. These can then be used to adjust the *boundary conditions* within OpenFOAM.

#### Results

After all parameters are set, the solver we can start the solver. When finished, we want to store the *results* of a scenario in the database. First of all, this means storing the results of every scenario numerically. After weighing the results using the occurrence of each wind direction, the sum of the weighted results is stored for every scenario group.

Furthermore, it would be of added value to store a *raster* version of the results directly into the database using PostGIS. This would enable us to visualise the results quickly in GIS software.

### 5.1.2 UML diagram

The analysis of the database requirements led to an initial data model in the form of unified modeling language (UML) class diagram (figure 5.2). UML is a visual modelling language that is often used to design and understand data models. The UML diagram is used to model the data requirements and behaviour of objects (Abraham

Kelilo Tula & Firaol Befikadu Geleta, 2019). In the diagram, different types of data classes are shown, along with the relationship between them. The diagram acts as an outline for the database design later on.

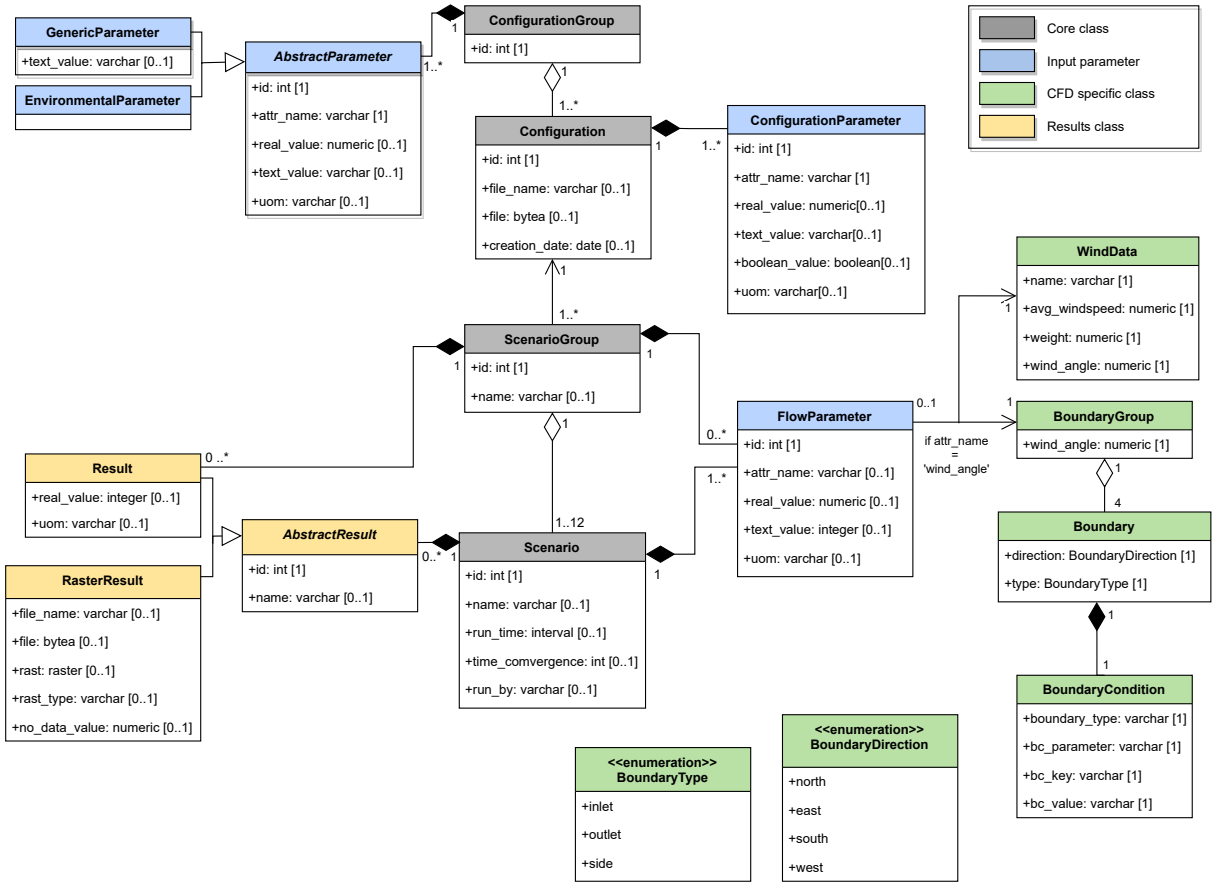


**Figure 5.2.** UML class diagram

The classes in the UML diagram can be divided into four main groups, (1) the core classes, (2) the input parameters, (3) the CFD specific classes and (4) the results classes. The core classes are subdivided into four classes. A configuration group consist of one or more configurations that are varied by changing one parameter at a time. One configuration is based on a series of configuration parameters. In the configuration class, all the metadata of the configuration and the 3D files themselves can be stored. In every configuration, there can be one or more scenario groups. One group consists of twelve different scenarios, one for every wind direction. The scenario group class is not of much use for this thesis, but this could be of added value in future use. Within the scenario class, all metadata of every scenario is stored. For every scenario and scenario group, the wind flow is defined by several flow parameters. The CFD specific classes contain information about wind flow based on the KNMI dataset (KNMI, 2019), and the corresponding boundary settings for CFD simulations. Lastly, the result classes store the resulting values for all scenarios and weighted results for the scenario groups. Furthermore, within the raster result class, georeferenced raster data can be stored.

### 5.1.3 Database design

The UML diagram is used as a base for the generation of the PostgreSQL database. Based on the diagram, we generated twelve tables in the PostgreSQL database. A complete overview of the database tables is shown in appendix B.2. This figure shows a complete entity-relationship diagram of the database, such as all the columns defined in the tables. Furthermore, the diagram includes the connections between tables and constraints, such as primary keys and foreign keys. PostgreSQL supports storage of binary files in ”Byte” format (Abraham Kelilo Tula & Firaol Befikadu Geleta, 2019). This means we can store the 3D STL files of every configuration and the tiff files containing the results directly into the database. Other file types are not stored directly into the database

but reference by name and location.

With the use of PostGIS and raster2pgsql tool, the georeferenced rasters are also stored in the database directly. This enables the user to open the rasters in GIS software.

### 5.1.4 Implementation

When finished running all the simulations, the database makes it easy to compare different elements. Using select queries within the databases enables the user to pick the factors to compare with each other. Examples of comparison that will be used:

- Sediment transport on the beach with and without houses
- Comparing varying wind conditions
- Comparing several beach house configurations

The comparisons are made using SQL select queries to retrieve the results from the database. Two examples of such queries are shown below. The first example is to retrieve scenario group results from the database, the second to retrieve the results van scenarios individually.

```
SELECT real_val
FROM openfoam.result
WHERE result_name = 'insert_result_name'
AND scen_group_id = 'insert_group_id';

SELECT real_val
FROM openfoam.result
WHERE result_name = 'insert_result_name'
AND scen_id = insert_scen_id;
```

## 5.2 Automating the process

We automated the process to let OpenFOAM run many simulations with different configurations and settings in a row. The process from start to finish is visualised in a simplified way in figure 5.3. It all starts with a user who enters the parameters for the simulations in a JSON file. This JSON file is then read, and based on these parameters, the database will be filled with configurations, scenarios and groups.

In order to let OpenFOAM and PostgreSQL communicate with each other, we set up a Python script. The primary function of this Python script is to retrieve parameters for one scenario from the database and send this to OpenFOAM. Once OpenFOAM is finished with running the solver and doing the post-processing, the Python script retrieves the results and stores these back in the database. This process continues until all scenarios are finished.

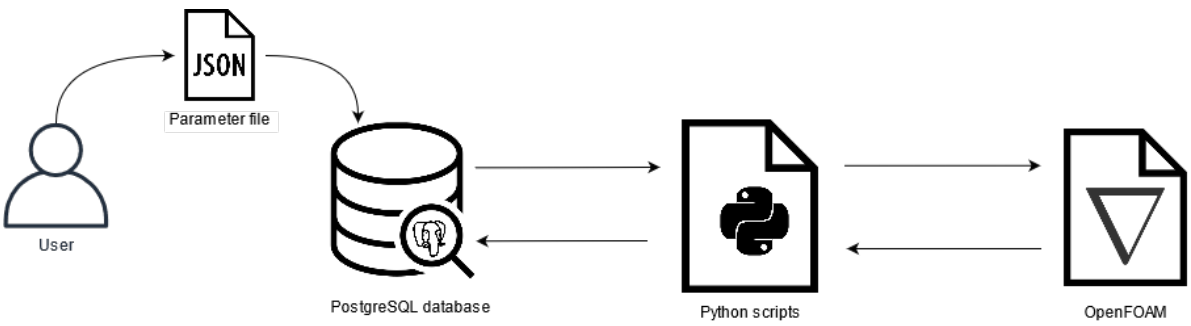


**Figure 5.3.** Simplified use case diagram

### 5.2.1 Python packages

For the collection and storage within the PostgreSQL database, we use the PsycoPg2 package. This package acts as an adapter between PostgreSQL and Python (Gregorio & Varrazzo, 2021). SQL queries can be executed directly from the Python code which makes it easy to retrieve and store data.

To adapt the OpenFOAM settings with Python we used the package PyFOAM. PyFOAM allows to adapt the OpenFOAM dictionary files and control the simulations. Other packages we used are the VTK and STL package, rasterio and some very common packages such as numpy and matplotlib.

### 5.2.2 Code structure

All the Python code together is divided over ten different files and consists of around 50 different functions. When the code has retrieved the parameters for a certain configuration from the database it can do everything from creating the 3D model and the mesh to georeferencing a tiff file.

To understand the basics of the Python code, we use a piece of pseudocode based on the main Python function that directs all other functions and processes (algorithm 5.1). This section shows how the code retrieves a list of configurations from the database and loops through all configurations within the list. For every configuration it generates a 3D model and a mesh. The mesh is then decomposed over a number of cores, to speed up the process of running the simulations.

It continues by retrieving a list of scenarios that correspond to a configuration from the database, and looping through the scenarios individually. For every scenario the code sets the correct parameters in OpenFOAM and starts the simulation. After the simulation has converged, the post-processing starts. This includes the analysis of the cutting plane and transformation to a georeferenced tiff file. As a last step the achieved results are stored back in the database and code continues to the next scenario until all are done.

**Algorithm 5.1:** Loop

```
1  select configuration_id from database as list_configurations ;
2  for configuration in list_configurations do
3      create 3D model ;
4      create mesh ;
5      decompose ;
6      select scenario_id from database where configuration_id is configuration as list_scenarios ;
7      for scenario in list_scenarios do
8          set OpenFOAM ;
9          run solver ;
10         post-process ;
11         store in database ;
```

# 6

# Results and Analysis

This chapter shows the results from the CFD simulations. We begin with comparing the results of a group of simulations without any houses, as a baseline measurement, to simulations of a situation with four beach houses. Secondly, we look at the varying impact of the different wind conditions on the dune ward sediment transport. The following comparison is between the different beach house configurations using weighted annual values per wind direction. This comparison can show the effects of every configuration on the dune-ward sediment transport. Lastly, we compare the results of all configurations and test the connection between sediment transport and the wind facing surface of every configuration (section 4.4.2).

It is difficult to determine where the transported sediment will end up exactly, as this depends on many factors (section 2.1). For this reason, we compare the different scenarios based on the amount of transport directed towards the dunes. To do this, we look at the following two values:

1. The average dune-ward sediment value at line x = 120 m. This is the top of the first dune (figure 4.2 and 6.1). The reasoning being that all sediment that crosses this line will likely end directly in the dunes and can therefore aid in dune formation. The higher the value of this dune-ward sediment transport, the more sand per meter beach width per time step moves to the dunes.
2. The area before the line x = 120 m, where there is no dune-ward sediment movement. The motive behind determining this area is that we can estimate the beach's surface that is blocked from the wind by the beach houses. The smaller the area blocked by the houses, the better for the sediment transport.

For both of these values, we only take the measurements between y=25 m and y=225 m into account, as the values near the edges of the computational domain are prone to errors. These errors occur because the ground surface varies in height along the sides of the computational domain perpendicular to the shore (figure 4.2).

## 6.1 Sediment transport with and without beach houses

Starting, we look at the dune-ward sediment transport on a 3D model without any houses as a baseline measurement (BM). We compare this with a model containing four beach houses in a straight line (configuration group 1A). Each of the two 3D models is simulated twelve times for every wind direction and corresponding wind speed (table 4.4). The results of these simulations are shown in figure 6.1.

In figure 6.1 we can see that the sediment transport in the empty model is generally higher than in the model with beach houses. This difference is noticeable from the SSW direction to the N direction, in clockwise order. These are the directions where the wind is blowing towards the dunes. If we look at the weighted annual values in table 6.1 the model without has, on average, 1.87e-6 kg/m/s more dune-ward sediment transport. This might not seem much, however, this converts to around 32 kg sediment transport per day along the beach section of 200 meters that we measured. This adds up to around 7000 kg when considering that the beach houses stand on the beach for seven months.

Table 6.1 shows that with some of the wind directions, the dune-ward sediment transport is higher, and the area without movement smaller in the model with houses. This might seem counterintuitive, however, we expect

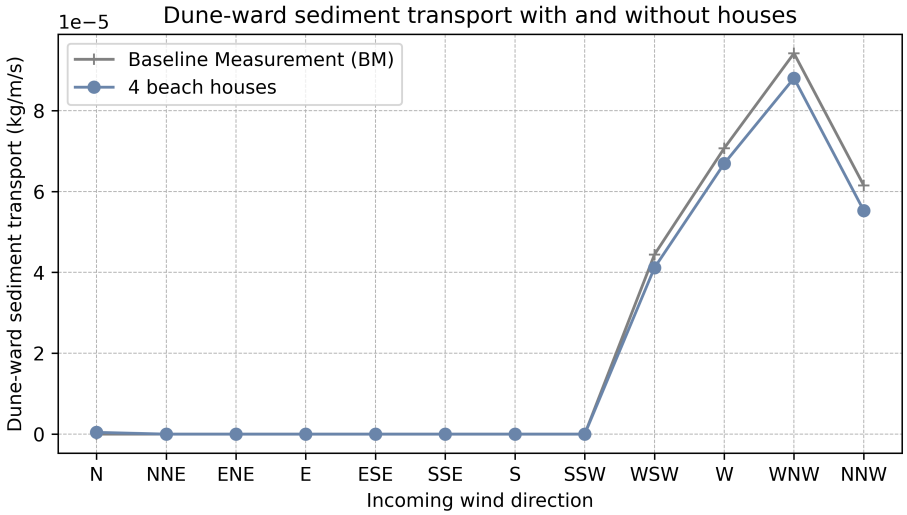


**Figure 6.1.** Dune-ward sediment transport on a beach with and without beach houses

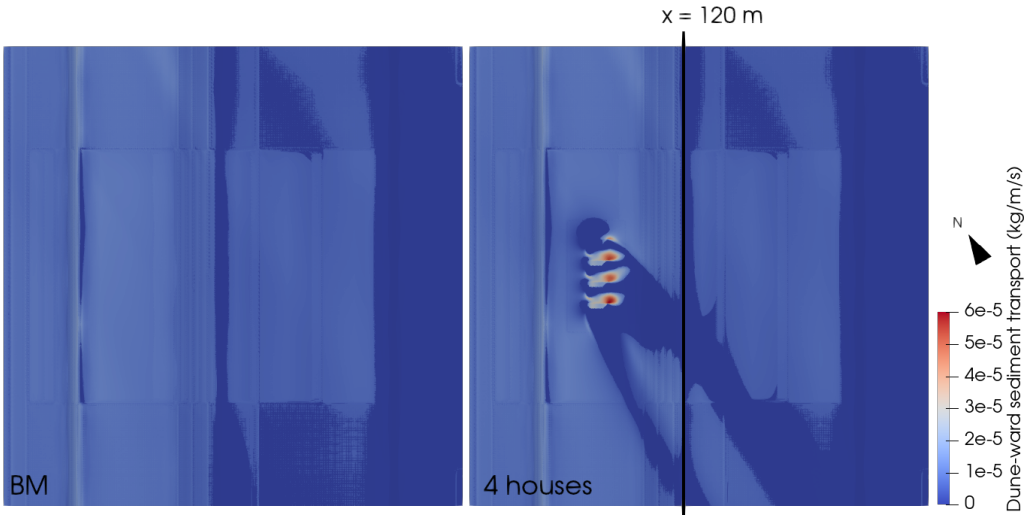


**Figure 6.2.** Dune-ward sediment transport in a model without (left) and with (right) beach houses, wind coming in from W

**Table 6.1.** Sediment transport and area w/o movement for a model with and without beach houses

| | *Dune-ward sediment transport (kg/m/s)* | | *Area without movement (m2)* | |
|---|---|---|---|---|
| **Wind direction** | **BM** | **4 houses** | **BM** | **4 houses** |
| N | 0 | 4.376E-07 | 375.24 | 1426.56 |
| NNE | 0 | 0 | 24157.32 | 24072.16 |
| ENE | 0 | 0 | 24160 | 24159.2 |
| E | 0 | 0 | 24160 | 24160.0 |
| ESE | 0 | 0 | 24160 | 24160.0 |
| SSE | 0 | 0 | 24160 | 24160.0 |
| S | 0 | 0 | 24160 | 24158.24 |
| SSW | 0 | 0 | 24146.76 | 22200.8 |
| WSW | 4.44E-05 | 4.115E-05 | 0.76 | 535.92 |
| W | 7.07E-05 | 6.692E-05 | 9.68 | 624.76 |
| WNW | 9.42E-05 | 8.804E-05 | 21 | 797.28 |
| NNW | 6.15E-05 | 5.529E-05 | 15.96 | 746.24 |
| Weighted total | 2.65E-05 | 2.457E-05 | 11172.64 | 11402.36 |

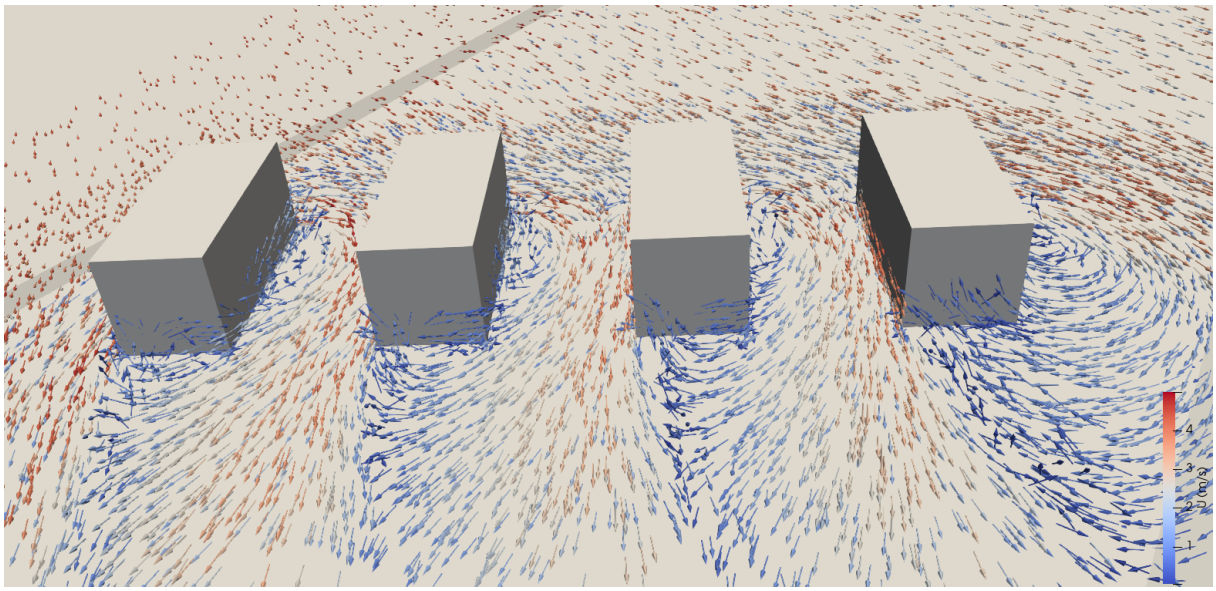

**Figure 6.3.** Airflow around beach houses

this is due to the interaction of the wind with the houses. Figure 6.3 shows how the wind changes direction when it comes into contact with the beach houses.

## 6.2 Effects of varying wind conditions

Next up, we look at the varying wind conditions and how they affect the dune-ward sediment transport differently. Figure 6.4 shows the wind speed around the beach houses from configuration group 1A and how this changes depending on the incoming wind direction. The lowest average wind speed is coming from the SSE direction, and the highest average wind speed from the WSW. The effects of these different wind conditions on the dune-ward sediment transport are shown in figure 6.5. This figure might seem off, but the wind coming from the dunes (NNE-SSW) naturally show very little to no dune-ward sediment transport, as the wind is blowing in the wrong direction. The majority of the sediment transport is generally due to the wind coming out of the WNW direction, pointing directly to the dunes and the WSW direction, which is the prevailing wind direction. In figure 6.5 the errors that occur near the edges of the computational domain are also visible.

## 6.3 Comparing different beach house configurations: group 1-3

Finally, we compare different beach house configurations and how they affect the dune-ward sediment transport differently. We start with comparing configuration group 1, 2 and 3.

### 6.3.1 Group 1: Changing the angle of a row of houses

Configuration group 1 consisted of four different configurations by changing the angle of the row of houses. Starting from 0°, parallel to the shore, the houses are rotated to 20°, to 40°, to 60°, towards the most common wind directions.

Figure 6.6 shows the results from the simulations with the wind coming from the WSW direction, as this is the prevailing wind direction. The figures show the amount of dune-ward sediment transport in kg/m/s. It ranges from red where the amount of transport is the highest, to blue where the amount of transport is low, to yellow where there is no transport at all.

Figure 6.7 and 6.8 comprise the weighted annual values for each of the four configurations, compared with the values from the empty model as the baseline measurement (BM). These figures would give a perspective of the

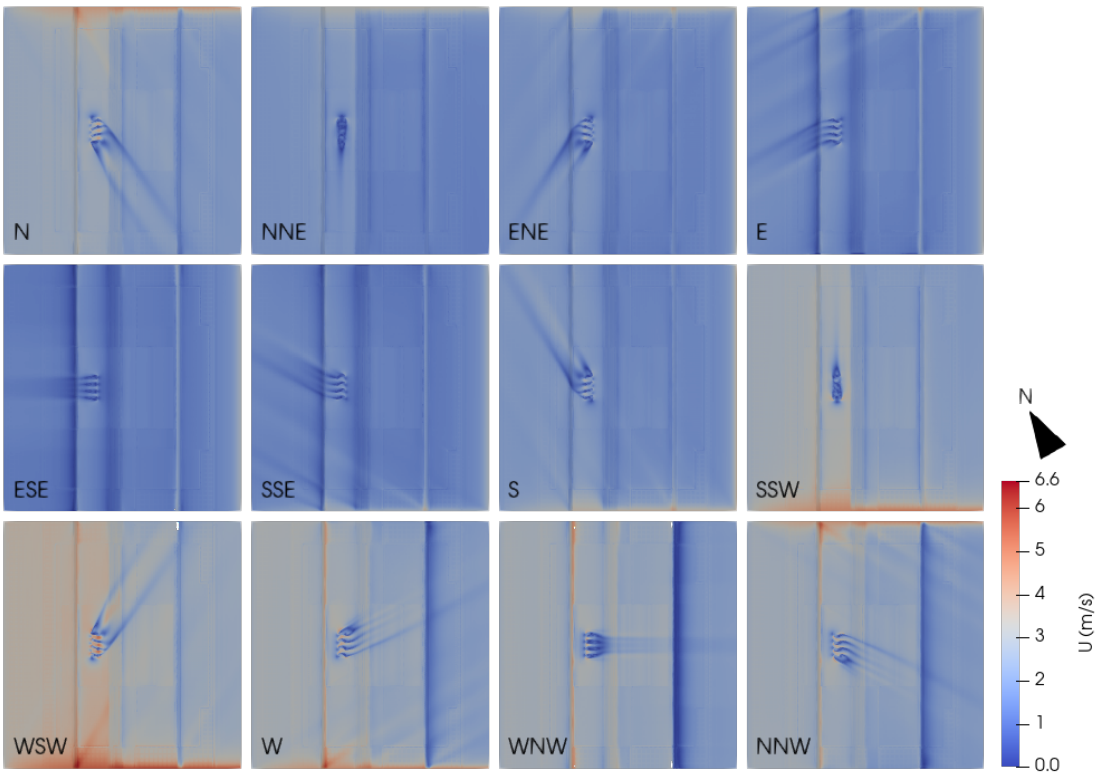


**Figure 6.4.** Wind speed at 0.3m height with varying incoming wind directions

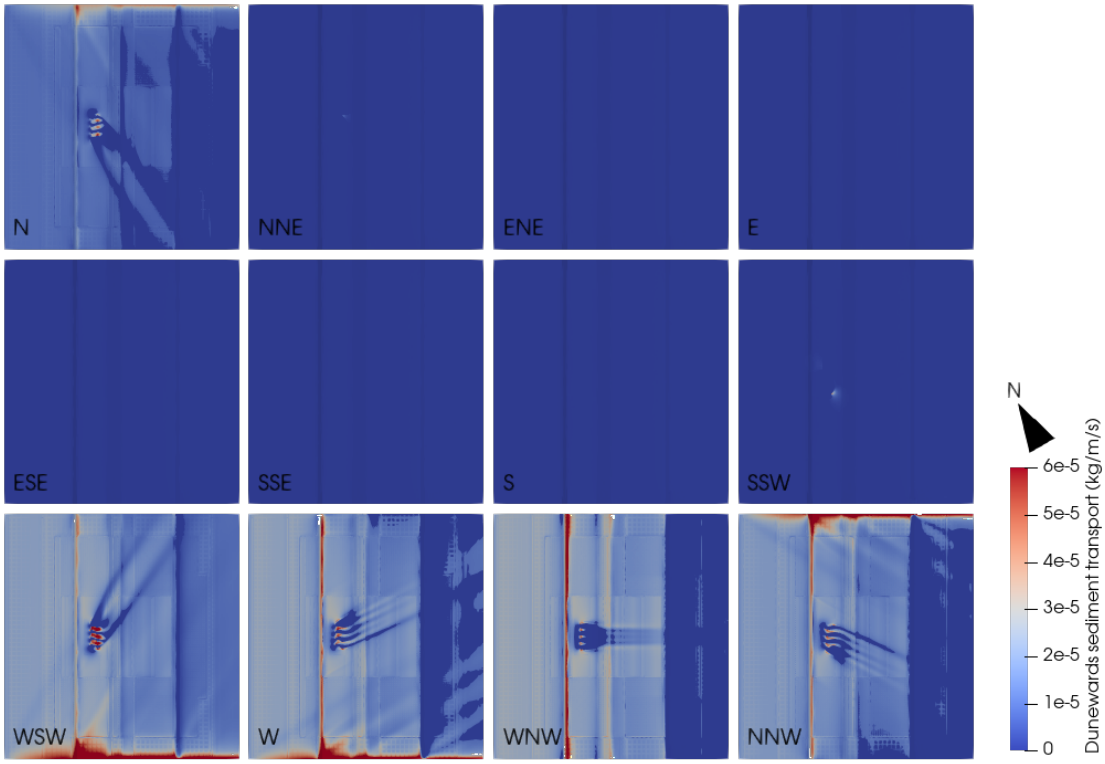


**Figure 6.5.** Dune-wards sediment transport at 0.3m height with varying incoming wind directions

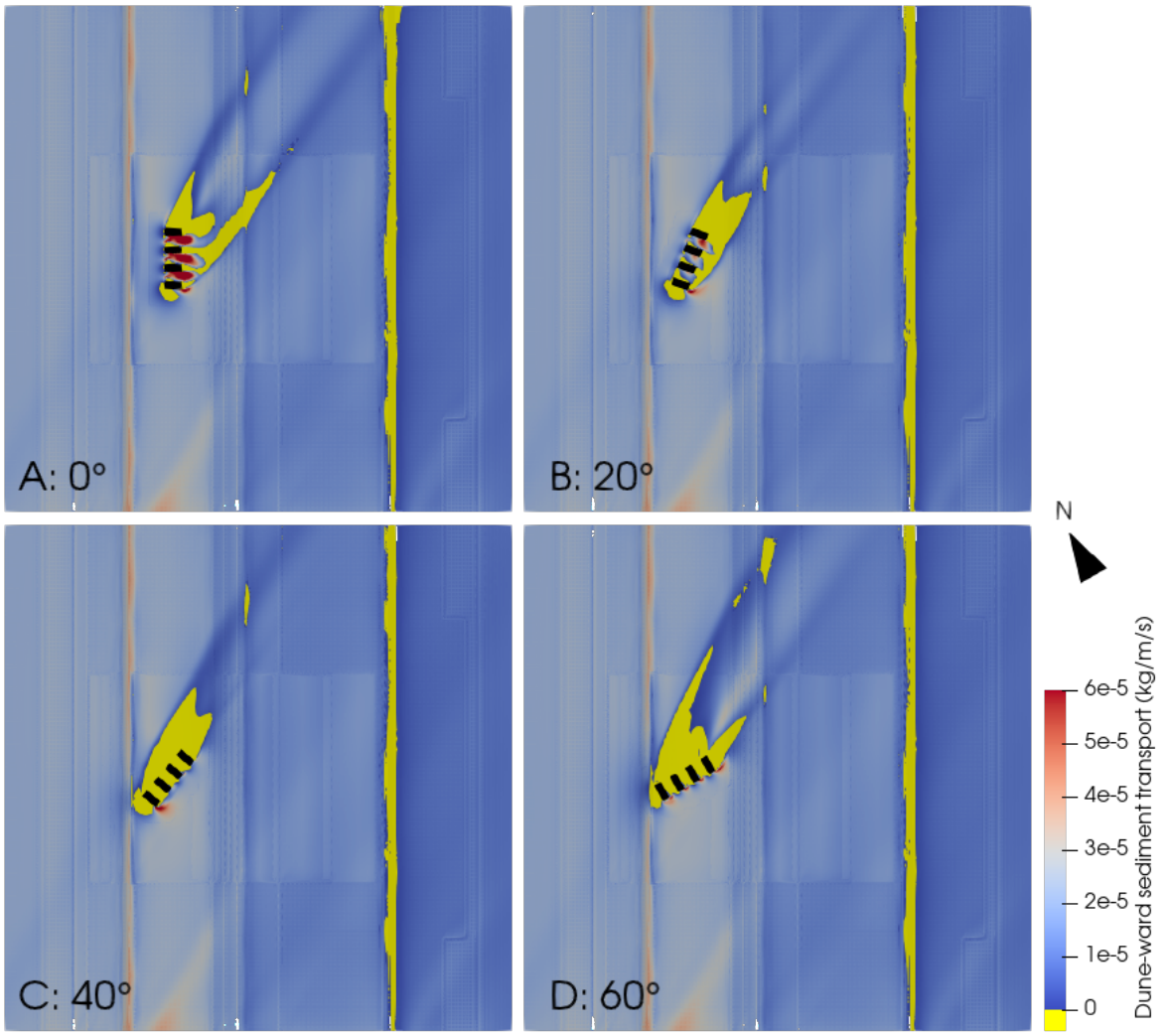


**Figure 6.6.** Configurations group 1: dune-ward sediment transport, wind coming from WSW

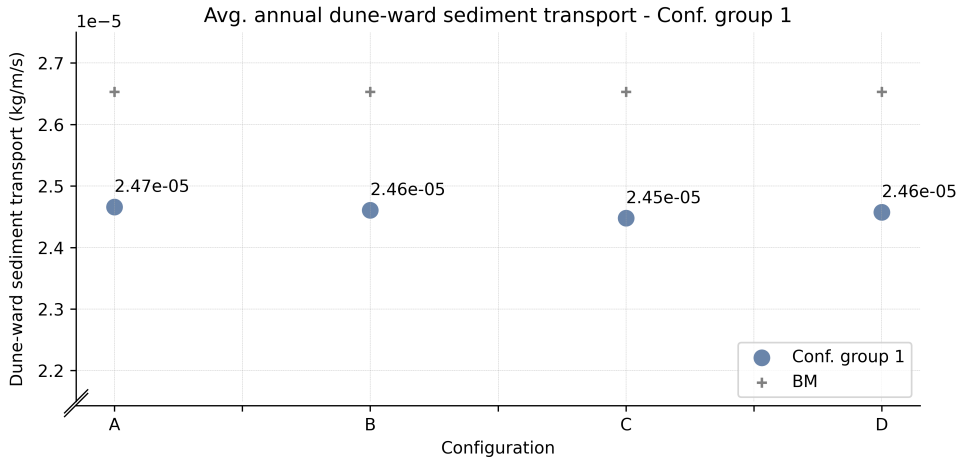


**Figure 6.7.** Configuration group 1: weighted dune-ward sediment transport crossing the top of the dunes. A: 0° rotation, B: 20° rotation, C: 40° rotation, D: 60° rotation

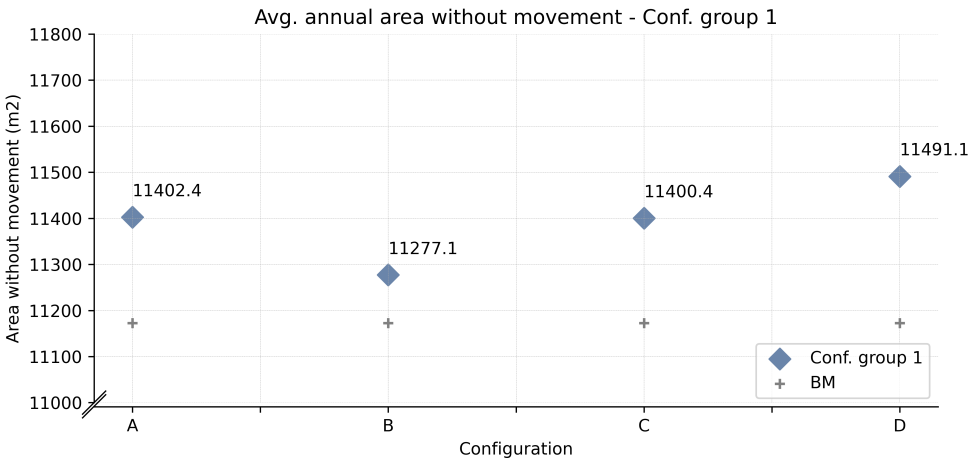


**Figure 6.8.** Configuration group 1: weighted areas without dune-ward sediment transport. A: 0° rotation, B: 20° rotation, C: 40° rotation, D: 60° rotation

average effect of the beach houses if they were placed on the beach for the whole season between April and October. The full results of the different configurations per wind direction can be found in appendix C.

Figure 6.7 shows that changing the angle of the row of houses seems to have little effect on dune-ward sediment passing the top of the first dune. Configuration C, with a row rotation of 40°, lowers the amount of sediment transport slightly compared to configuration A, with the houses parallel to the shore, but the difference is small. Figure 6.8 shows some more variation. Rotating the row of houses with 20° results in the smallest area without movement compared to the other configurations. This suggests that the area blocked by the houses in configuration 1B is the smallest.

### 6.3.2 Group 2: Changing the angle of houses individually

In configuration group 2, we look at the consequences of rotating the beach houses individually. Starting with each of the houses facing the sea as 0°, and turning the houses to 30°, 60° and eventually 90°. In figure 6.9 we see the dune-ward sediment transport for all four of the different configurations, again with the wind coming from WSW direction.

Based on figure 6.10 it seems that rotating the houses individually has more effect on the dune-ward sediment transport than rotating the whole row of houses. Rotating the houses 30° appears to increase the amount of dune-ward sediment transport. Rotating for more than 30° lowers the sediment transport by a considerable amount. Additionally, figure 6.11 shows the results when it comes to the area without sediment movement. Rotating the houses 30° to 60° towards the prevailing wind seems to lower the stationary area. Whereas rotating the houses 90° increases the area without movement largely.

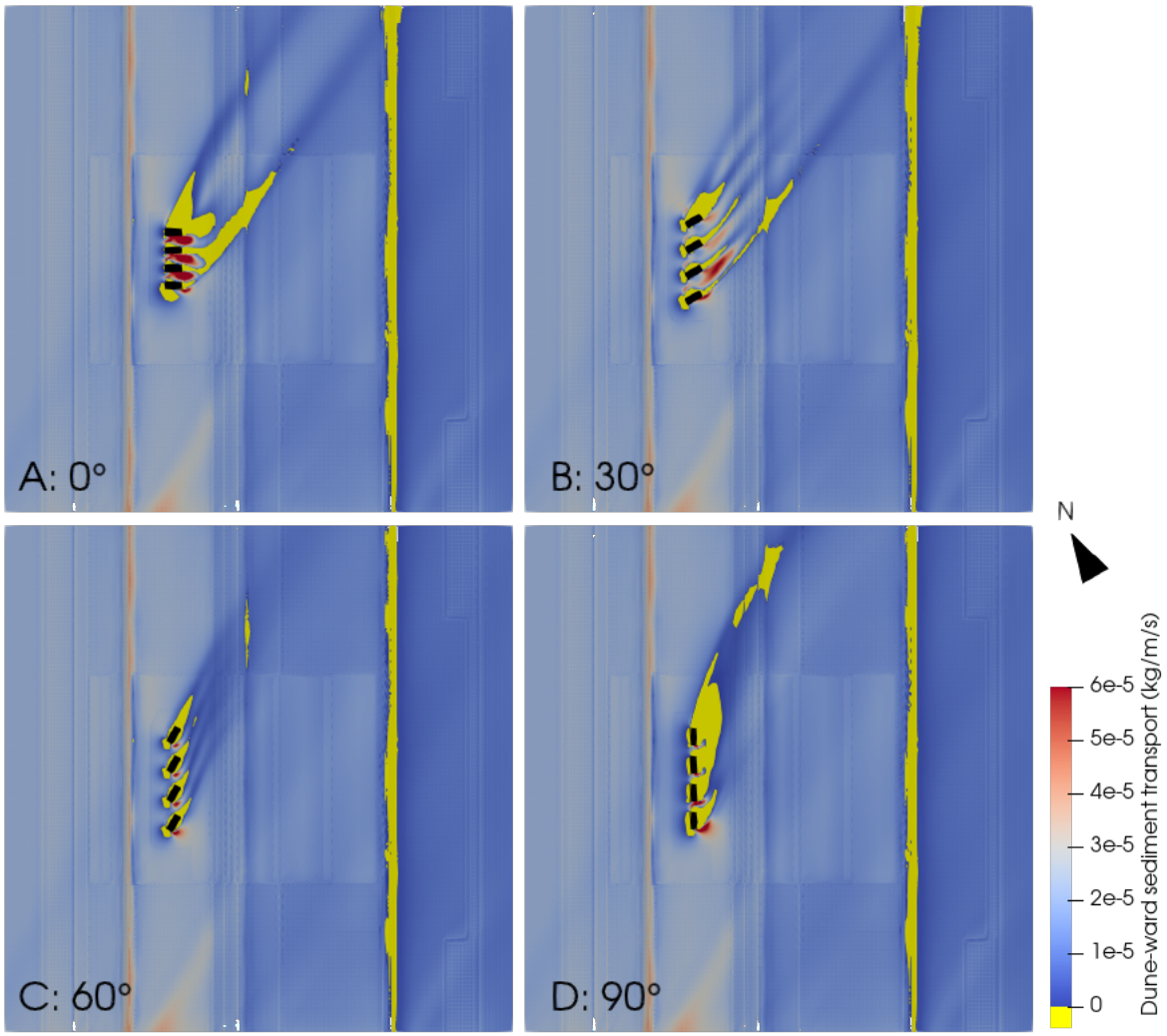


**Figure 6.9.** Configurations group 2: dune-ward sediment transport, wind coming from WSW

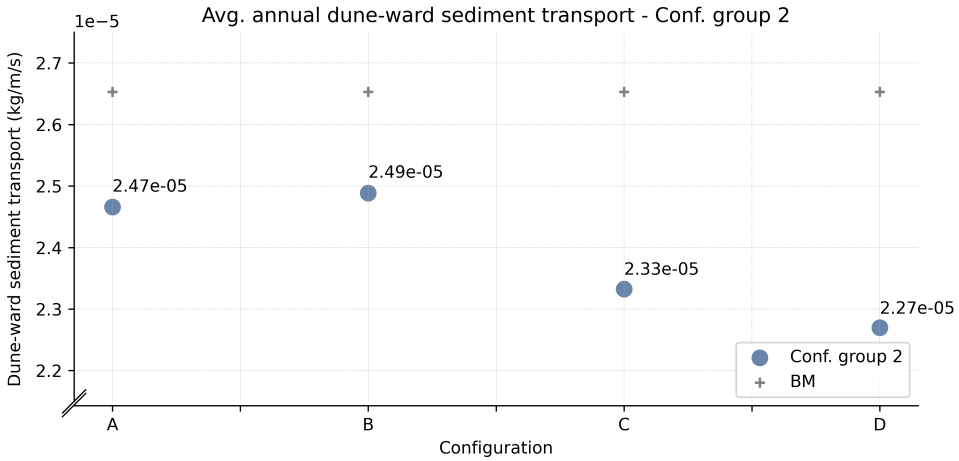


**Figure 6.10.** Configuration group 2: weighted dune-ward sediment transport crossing the top of the dunes. A: 0° rotation, B: 30° rotation, C: 60° rotation, D: 90° rotation

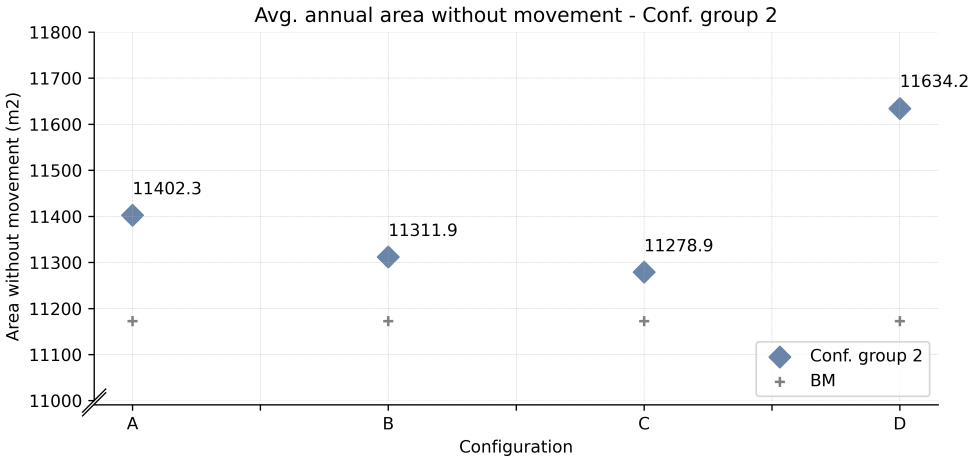


**Figure 6.11.** Configuration group 2: weighted area without dune-ward sediment transport. A: 0° rotation, B: 30° rotation, C: 60° rotation, D: 90° rotation

### 6.3.3 Group 3: Combining group 1 and 2

The third group of configurations is based on the results from the first two groups. The results from the first group of configurations show that rotating the row of houses for around 20 degrees seems to have a positive effect on the area without movement. The results from configuration group two suggest an increase in dune-ward sediment flow by rotating the houses towards the prevailing wind direction. These two results lead to the creation of the configurations in the third group. Here we combine rotating the row with 20° and study the changes when rotating the individual houses by 0°, 30°, 60° and 90°, similar to group 2. The idea behind this being that this will lower the size of the wind-facing surfaces.

Figure 6.12 shows that a combination of rotating a row of houses 20° and rotating them individually with 30° (configuration 3B) has the highest amount of sediment transport moving towards the dunes. Similar to group 2, rotating the individual houses more than 30° degrees lowers the amount of sediment transport. A similar conclusion can be drawn from figure 6.13, where 3B also shows the smallest area blocked by the beach houses. In fact, the area blocked by the houses is not far off from the baseline measurement without any houses.

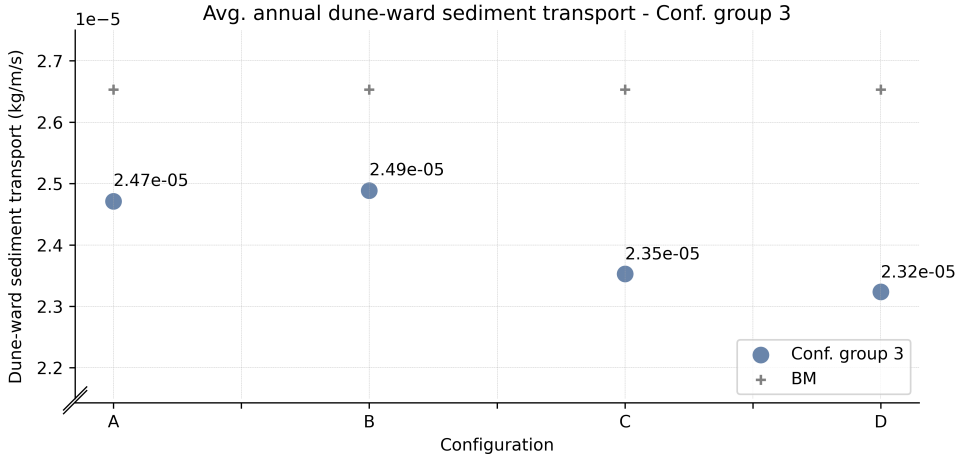


**Figure 6.12.** Configuration group 3: weighted dune-ward sediment transport crossing the top of the dunes. A: 0° rotation, B: 30° rotation, C: 60° rotation, D: 90° rotation

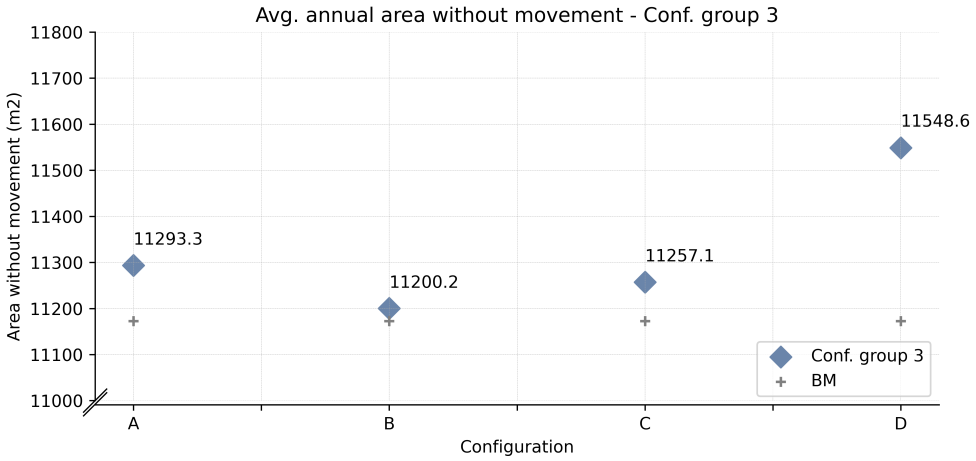


**Figure 6.13.** Configuration group 3: weighted area without dune-ward sediment transport. A: 0° rotation, B: 30° rotation, C: 60° rotation, D: 90° rotation

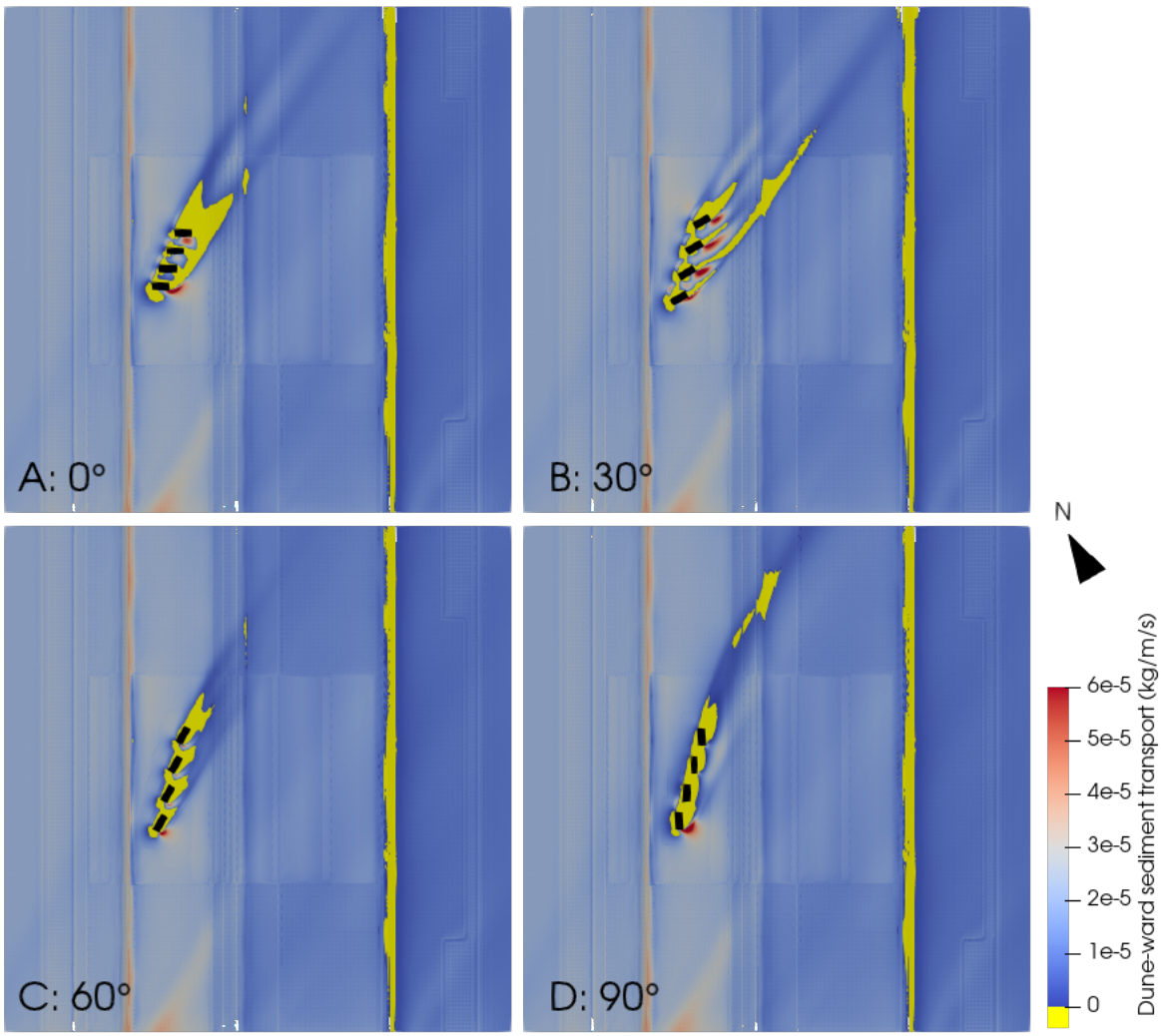


**Figure 6.14.** Configurations group 3: dune-ward sediment transport wind coming from WSW direction

The images in figure 6.14 show the dune-ward sediment transport for the four different configurations in group 3. They show wind coming from the WSW direction, which is also the direction in which the houses are pointed.

### 6.3.4 Evaluation of configurations 1-3

Table 6.2 and 6.3 show the weighted results of the group 1, 2 and 3 combined. The full results of the different scenarios can be seen in appendix C. Configuration 2B and 3B clearly show the best result when looking at the dune-ward sediment transport. This conclusion is confirmed when looking at the area without movement, as configuration 2B and 3B have the lowest stationary area. Configuration 3B shows slightly better results overall. The worst configurations in terms of both sediment transport and area without movement are configuration 2D and 3D.

**Table 6.2.** Combined results of the dune-ward sediment transport (kg/m/s)

| | A | B | C | D |
|---|---|---|---|---|
| **Group 1** | 2.466E-05 | 2.448E-05 | 2.461E-05 | 2.466E-05 |
| **Group 2** | 2.466E-05 | 2.488E-05 | 2.333E-05 | 2.270E-05 |
| **Group 3** | 2.471E-05 | 2.489E-05 | 2.353E-05 | 2.324E-05 |

**Table 6.3.** Combined results of the area without movement (m2)

| | A | B | C | D |
|---|---|---|---|---|
| **Group 1** | 11402.4 | 11277.1 | 11400.4 | 11491.1 |
| **Group 2** | 11402.3 | 11278.9 | 11311.9 | 11634.2 |
| **Group 3** | 11293.3 | 11200.2 | 11257.1 | 11548.6 |

## 6.4 Comparing different beach house configurations: group 4-5

Configuration group 4 places the houses in stair-like shapes. Figure 6.16 shows the results of the dune-ward sediment transport for the three configurations in group 4. The graph in figure 6.15a shows that both configuration 4A and 4C show an increase in dune-ward sediment transport compared to configuration 4B, with the houses in a straight line. Furthermore, both star-shaped configurations show a definite decrease in the stationary area. Mainly configuration 4C is interesting to study further as this shows the highest dune-wards sediment value.

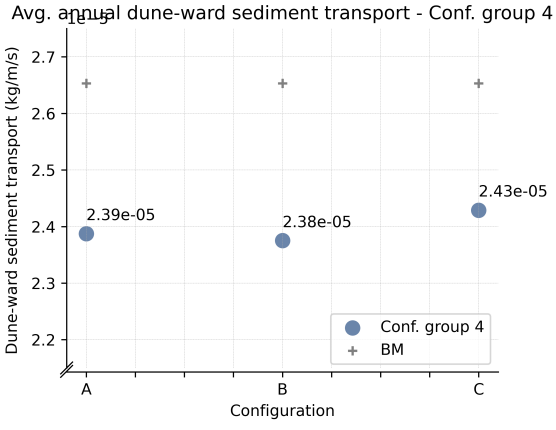


(a) Weighted dune-ward sediment transport crossing the top of the dunes

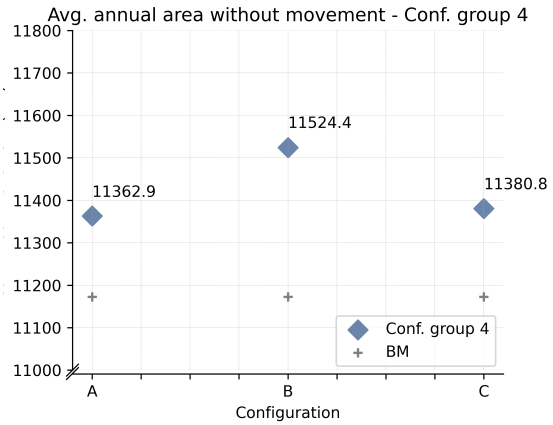


(b) Weighted area without dune-ward sediment transport

**Figure 6.15.** Weighted results configuration group 4

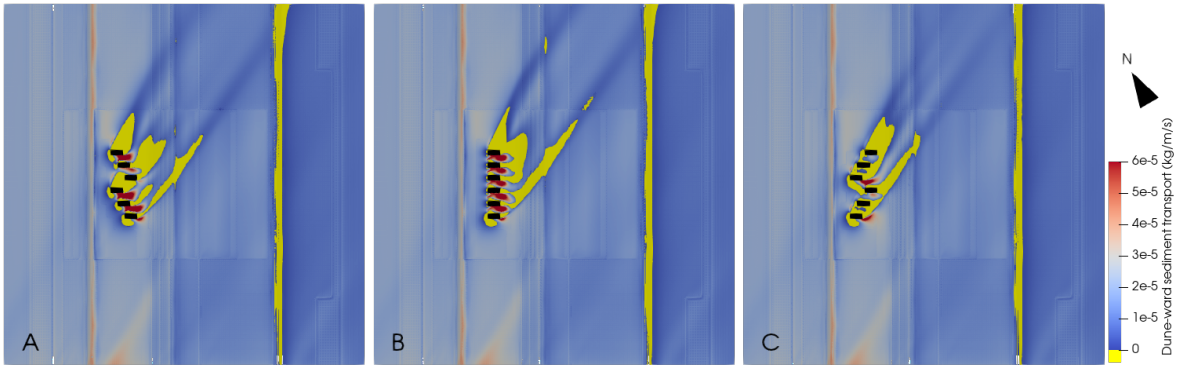


**Figure 6.16.** Configurations group 4: dune-ward sediment transport wind coming from WSW direction

Configuration group 5 introduces the v/funnel shape. Configuration 5A has a v-shape pointing towards the sea and 5C pointing towards the dunes. In configuration 5B, the houses are in a straight line and act as a comparison. Looking at figure 6.18a configuration 5A and 5C both show improvements in the amount of sediment transport compared to 5B. Both 5A and 5C also show a decrease in the area without movement. Configuration 4C and 5C show the best results overall, as both lead to an increase in sediment transport and a decrease in stationary area.

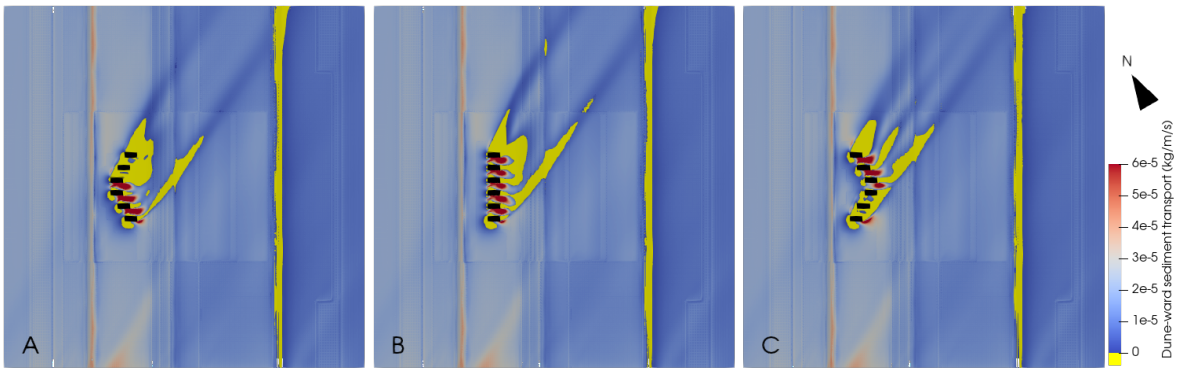


**Figure 6.17.** Configurations group 5: dune-ward sediment transport wind coming from WSW direction

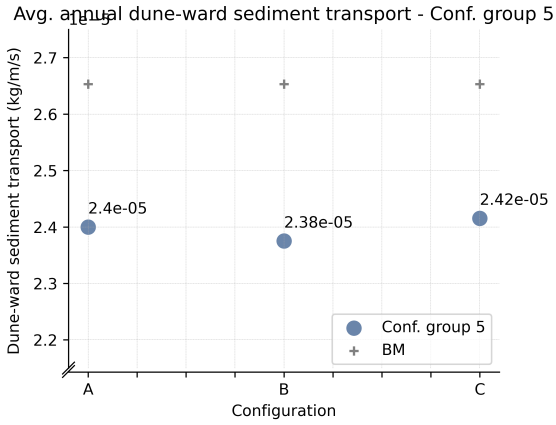


(a) Weighted dune-ward sediment transport crossing the top of the dunes

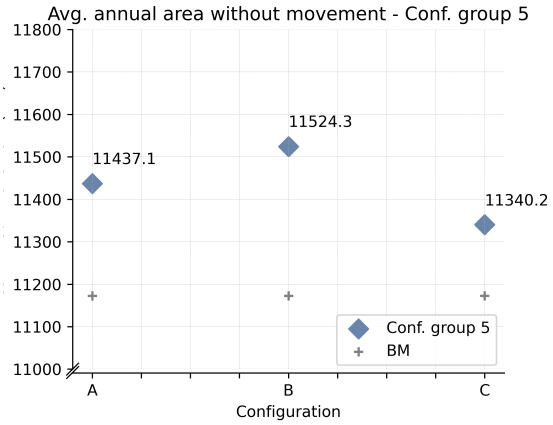


(b) Weighted area without dune-ward sediment transport

**Figure 6.18.** Weighted results configuration group 5

### 6.4.1 Aiding in dune formation

Although changing the configurations of the beach house makes a difference in the amount of dune-ward sediment transport, it is difficult to determine if these configurations can aid dune-formation directly. By placing the houses in specific ways, the amount of blockage caused by the houses can be limited. However, the beach houses still cause less sediment transport than in a scenario without any beach houses, like the baseline measurement. Furthermore, as stated earlier, the exact location of the sedimentation is very difficult to determine. This is dependent on many more factors, such as the vegetation, the slope of the dunes and the wind blowing in the -wrong- seawards direction.

## 6.5 Relationship between wind facing surface and dune-ward sediment transport

Lastly, we look at the relationship between the wind facing surface and the amount of dune-ward sediment transport. To do this, we compare the results of all 16 configurations that are discussed so far. Figure 6.19 shows the wind facing surface of all configurations on the x-axis and the weighted dune-ward sediment transport on the y-axis. We can draw a trend line that shows a slight negative correlation, which means that a smaller wind facing surface shows a somewhat higher amount of dune-ward sediment transport. However, the level of correlation is quite low. The value of variation, $R^2$, is around 0.2.

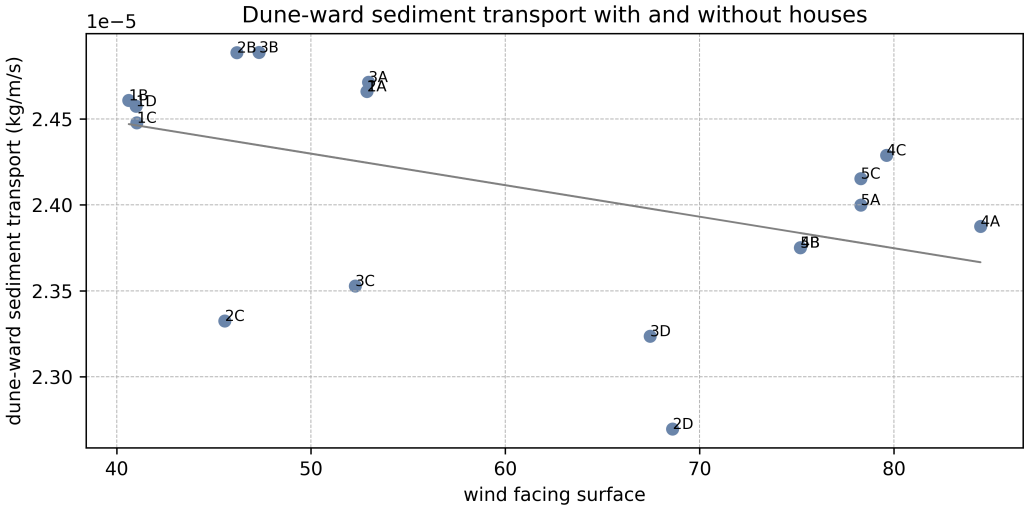


**Figure 6.19.** Wind facing surface and dune-ward sediment transport

# 7 Discussion

## 7.1 Limitations of the CFD models

When creating computer-generated simulations, there will always be some adaptions compared to the real world. To run many different simulations in a relatively short amount of time, we simplified the model compared to reality in several ways.

First of all, we assume that sediment transport is only influenced by wind speed, wind direction and particle size. In reality, many more factors influence sediment transport. Moisture, fetch distance and different sediment characteristics could be taken into account to predict the sediment transport more accurately (Delgado-Fernandez, 2011). Previous studies show that without these limiting factors, the sediment transport is often overestimated compared to reality (Delgado-Fernandez, 2011). In this research, we simplified the sediment transport by assuming these factors would be stable during all scenarios. This might not give the most accurate absolute results when it comes to the predicted sediment transport. This simplification does, however, make it easy to compare the different scenarios with each other.

Furthermore, the 3D model based on a section of Noordwijk beach is also a simplification of reality. The dunes are, for example, much more complex than modelled in this thesis. Besides, the beach is not nearly as smooth as modelled, and the width changes along with the tides.

## 7.2 Assessment of the results

There some limitations to the OpenFOAM settings we used to run the simulations. First of all, using the RANS method to solve the Navier-Stokes simulations can result in uncertainties (García-Sánchez et al., 2017). These uncertainties might affect the turbulence as well as the boundary conditions (Lamberti et al., 2018). Using LES instead of RANS can simulate the turbulence much more realistically as the largest turbulent eddies are resolved rather than modelled (Blocken, 2014). A disadvantage of using LES is, however, that it takes a lot more computation time and power (Blocken, 2014).

Lastly, while running the simulations, there were some issues with reaching convergence, specifically for the scenarios with the wind coming from the south-east-east direction. This is the direction where the wind comes straight from the dunes and blows towards the sea. The error seems to depend on some of the initial boundary settings. Changing those settings and improving the mesh helped for the majority of simulations. However, some scenarios still had trouble with convergence. So far, we have not been able to eliminate it completely. On the other hand, the wind coming from the SEE direction often does not occur, and the average wind speed is low. Combining this with the fact that the wind is blowing from the dunes, we assume the effect of this wind direction on the dune-ward sediment transport is negligible.

Furthermore, we question the way we performed the analysis of the results. Determining the amount of sediment transport crossing the top of the first dune might not accurately represent what is happening in the area in front of the dune. The area without movement does do that but does not consider the differences between amounts of sediment transport.

## 7.3 Feasibility of configurations

In a more practical sense, not all beach house configurations are realistic to be built. Placing the houses closer to the sea limits the width of the beach for recreational use. Furthermore, there needs to be enough space left for emergency vehicles to access the beach, even during high tide. This is a factor we need to take into account for multiple of the beach house configurations.

Moreover, when rotating the beach houses towards the prevailing wind conditions, we need to take the direction of the entrance doors and outside seating area of the houses into account. Placing the doors and seating area directly facing the prevailing wind can be uncomfortable for the guests of the beach houses. Similarly, when rotating the houses, the houses point towards each other more than would be the case with the house perpendicular to the shore. Therefore we need to consider the level of privacy of the guests.

## 7.4 Future work

For future work, we suggest improving the credibility of the results. First of all, by determining a way to analyse the results and rate the performance of every configuration accordingly. It would be of added value to having more configurations to compare with to get more detailed results of the effects of different configurations on sediment transport. Furthermore, using the most promising configurations in real-life measurements would be very interesting to validate the predictions made in this thesis.

Lastly, it would be useful to expand research on using database systems for storage of CFD-like data. Very little information was available on this and not many studies seem to implement a DBMS to keep track of different scenarios. For this research it provided a way of storing all necessary data in an organised way and made comparison later easy to do. The data model made for this thesis is a simple one however, and there is room for improvement and expansion.

# 8

# Conclusion

The main research question as defined in the introduction is *What are the effects of different beach house configurations on dune-ward sediment transport?*. The question can be resolved by answering the following sub-questions:

*What are the effects of the changing seasonal wind conditions on dune-wards sediment transport according to CFD simulations?* The CFD simulations show that the beach houses do indeed have a limiting effect on the wind flow moving across the beach. This also leads to a decrease in the dune-ward sediment transport. This is particularly noticeable for winds coming in from the West-South-West to West-North-West, as these wind directions are the most prevalent, have a high average wind speed and face the dunes directly.

*How do different beach house configurations compare in regards to dune-ward sediment transport?* Changing the angle of the row of beach houses shows minor effects on the dune-ward sediment transport. Rotating the house by 20° towards the prevailing wind directions limits the area without movement somewhat. The limitation of increasing the angle of the row of houses is that it takes up much space, which might not be desirable. Rotating the houses individually does not have this disadvantage. Turning the houses 30° to 60° towards the prevalent wind directions shows positive changes by increasing the amount of dune-ward sediment transport and limiting the stationary area behind the beach houses. Combining a row rotation of 20° and an individual rotation of 30° showed a slight improvement compared to the individual rotation alone. Placing the houses in a stair-like shape or v-shape pointing towards the dunes also shows the potential of increasing the total amount of sediment transport. However, here we also need to consider that enough space on the beach is left for accessibility. More tests are necessary to determine if these configurations aid the total amount of dune-wards sediment transport.

*What are the potential effects of beach house configurations on sedimentation and dune formation?* It is complicated to determine precisely where the transported sediment will end up and where sedimentation will occur, as many factors influence this. There are certainly ways in which the configurations can be placed that limit the dune-ward sediment transport a lot less compared to the traditional way the houses are placed, perpendicular to the shore. In some situations where the wind moves parallel to the shore, the beach houses even seem to have a small added effect. As the wind comes in contact with the houses, it can change direction and shift towards the dunes instead. This way, it can add to the total amount of dune formation. Compared to other wind directions where the houses block the transport going to the dunes, this effect is limited.

To get more insights into the effects of the beach house configurations, we recommend an improvement in OpenFoam settings used, test more types of configurations, and study the beach house configurations in real-life research. The results of this thesis can hopefully help ShoreScape in determining what scale models to try next during real-life beach measurements.

# A

# Site visit

(a) Noordwijk beach


(b) Beach houses on Noordwijk beach

(c) Beach houses

(d) Beach houses from the back

(e) Dune-foot

(f) Trying to make a photo of the aeolian processes

(g) Beach as seen from the dunes

(h) Beach and sea from the dunes

**Figure A.1.** Visiting the site of the beach in Noordwijk in the beginning of May 2021

# B

# Extra figures

## B.1 Grasshopper model

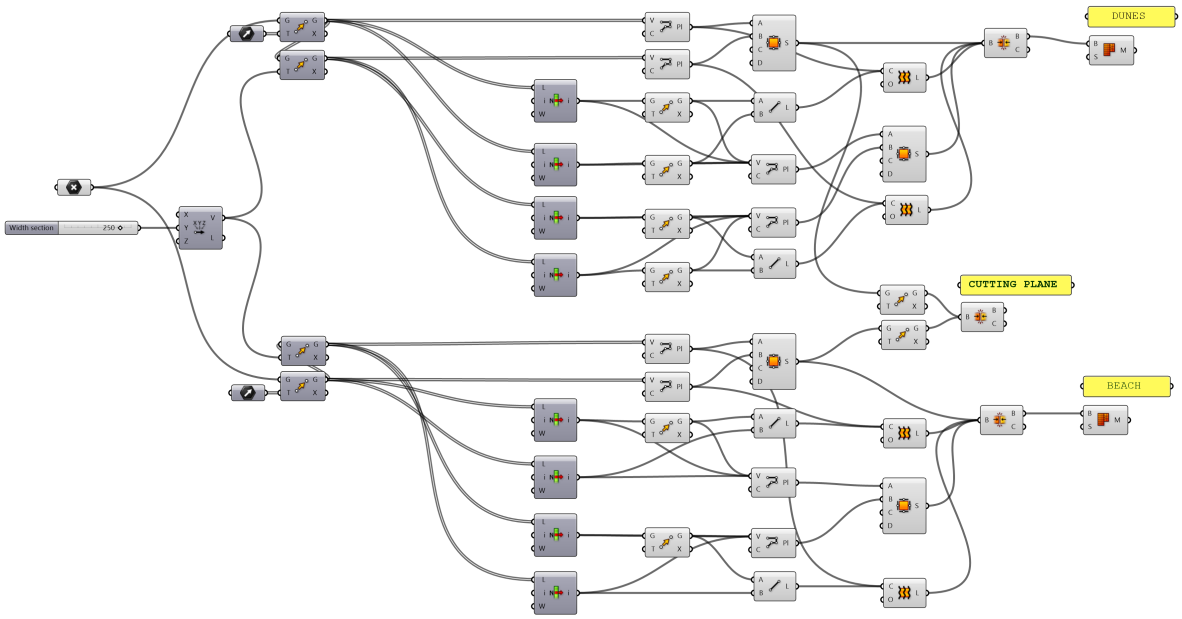


**Figure B.1.** Grasshopper model

## B.2 Entity relationship diagram

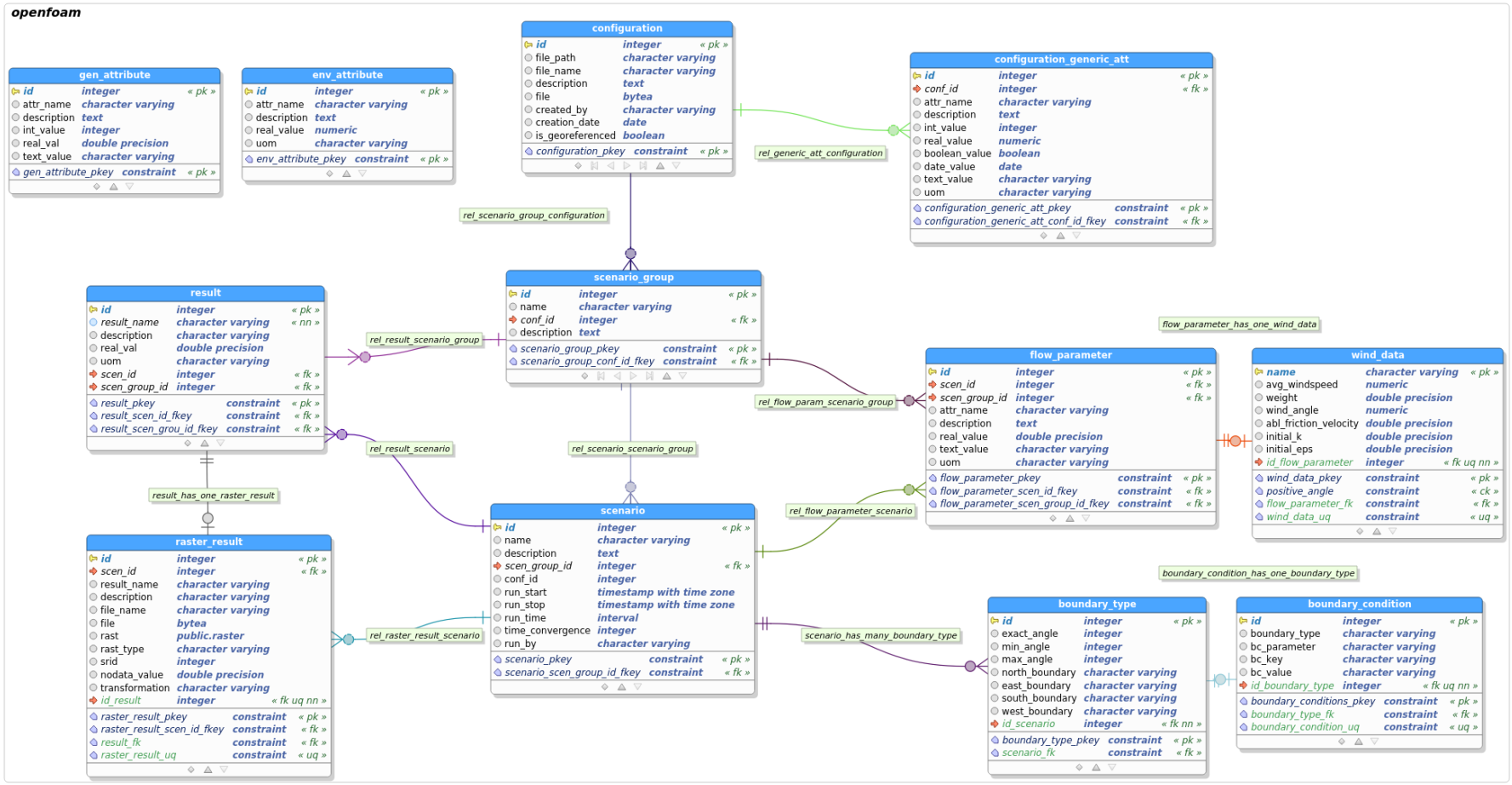


**Figure B.2.** Entity relationship diagram

# C

# Extended results

## C.1 Results baseline measurement

**Table C.1.** Results baseline measurement

| Wind direction | *Dune-ward sediment transport (kg/m/s)* | *Area without movement (m2)* |
|---|---|---|
| N | 0 | 375.24 |
| NNE | 0 | 24157.32 |
| ENE | 0 | 24160 |
| E | 0 | 24160 |
| ESE | 0 | 24160 |
| SSE | 0 | 24160 |
| S | 0 | 24160 |
| SSW | 0 | 24146.76 |
| WSW | 4.44205E-05 | 0.76 |
| W | 7.07137E-05 | 9.68 |
| WNW | 9.41755E-05 | 21 |
| NNW | 6.15173E-05 | 15.96 |
| Weighted total | 2.6532E-05 | 11172.64 |

## C.2 Results configuration group 1

**Table C.2.** Results group 1

| Group 1 | *Dune-ward sediment transport (kg/m/s)* | | | | *Area without movement (m2)* | | | |
|---|---|---|---|---|---|---|---|---|
| **Wind direction** | **A** | **B** | **C** | **D** | **A** | **B** | **C** | **D** |
| N | 4.376E-07 | 0 | 0 | 0 | 1426.56 | 1497.56 | 1589.52 | 1867.32 |
| NNE | 0 | 0 | 0 | 0 | 24072.16 | 23875.28 | 23857.48 | 24045.16 |
| ENE | 0 | 0 | 0 | 0 | 24159.2 | 24157.92 | 24138.2 | 24099.6 |
| E | 0 | 0 | 0 | 0 | 24160 | 24160 | 24160 | 24160 |
| ESE | 0 | 0 | 0 | 0 | 24160 | 24160 | 24160 | 24156.92 |
| SSE | 0 | 0 | 0 | 0 | 24160 | 24160 | 24160 | 24160 |
| S | 0 | 0 | 0 | 0 | 24158.24 | 24154.28 | 24153.4 | 24155.6 |
| SSW | 0 | 0 | 0 | 0 | 22200.8 | 20476.68 | 21593.36 | 22356.8 |
| WSW | 4.115E-05 | 4.16834E-05 | 4.14E-05 | 4.03E-05 | 535.92 | 533.6 | 665.2 | 801.8 |
| W | 6.692E-05 | 6.69555E-05 | 6.58E-05 | 6.86E-05 | 624.76 | 661.32 | 691.28 | 461.76 |
| WNW | 8.804E-05 | 8.86101E-05 | 8.89E-05 | 8.9E-05 | 797.28 | 808.72 | 721.76 | 775.24 |
| NNW | 5.529E-05 | 0.000053774 | 5.38E-05 | 5.4E-05 | 746.24 | 888.64 | 968.8 | 786.68 |
| Weighted total | 2.457E-05 | 2.44769E-05 | 2.46E-05 | 2.47E-05 | 11402.37 | 11277.08 | 11400.39 | 11491.13 |

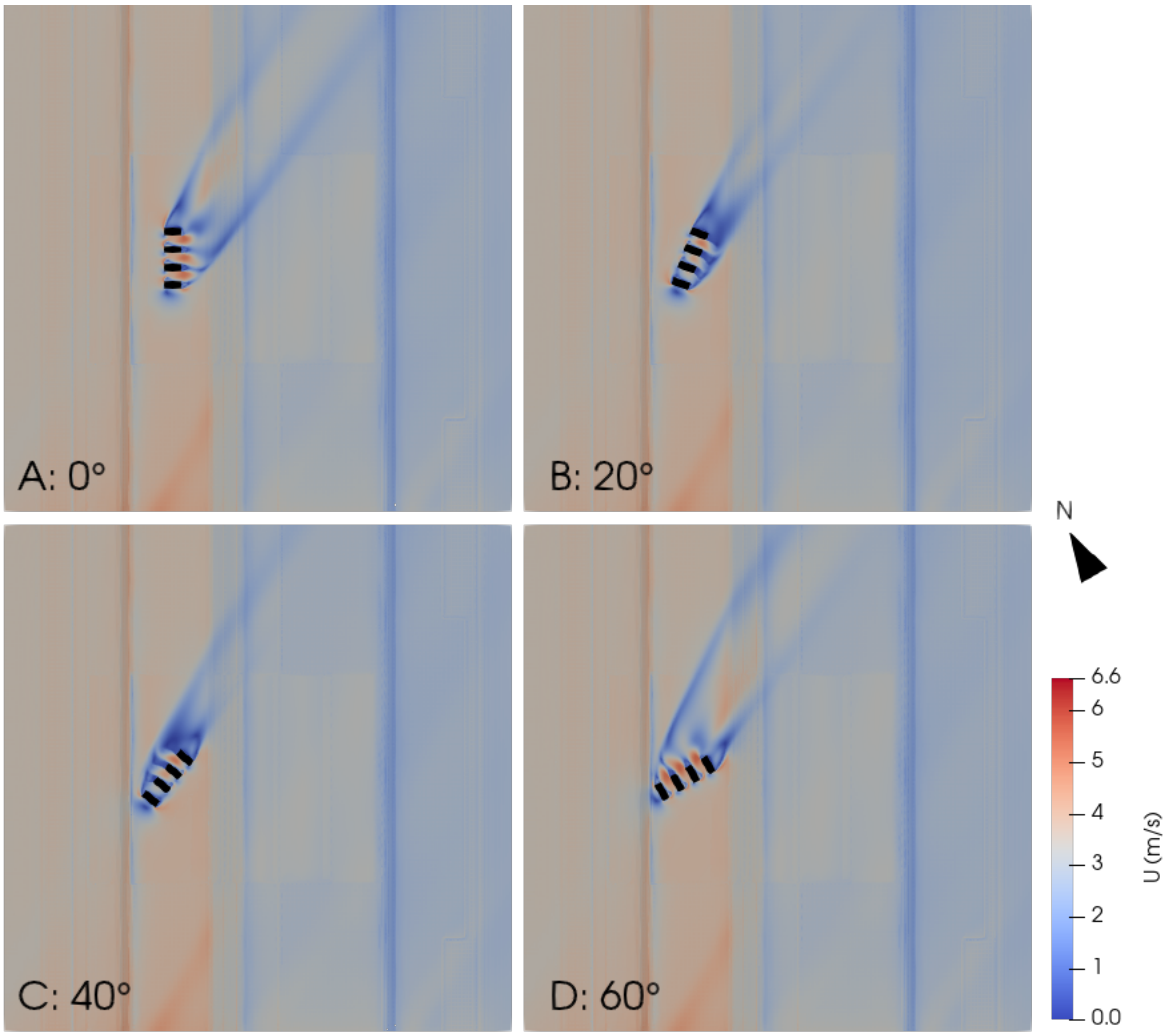


**Figure C.1.** Configurations group 1: wind speed - wind coming from WSW direction

## C.3 Results configuration group 2

**Table C.3.** Results group 2

| Group 2 | *Dune-ward sediment transport (kg/m/s)* | | | | *Area without movement (m2)* | | | |
|---|---|---|---|---|---|---|---|---|
| **Wind direction** | **A** | **B** | **C** | **D** | **A** | **B** | **C** | **D** |
| N | 4.376E-07 | 0 | 0 | 7.14E-07 | 1426.6 | 1895.72 | 2089.32 | 1476.96 |
| NNE | 0 | 0 | 0 | 0 | 24072.28 | 24064.48 | 24064.4 | 24080.96 |
| ENE | 0 | 0 | 0 | 0 | 24159.2 | 24154.32 | 24158.2 | 24158.96 |
| E | 0 | 0 | 0 | 0 | 24160 | 24160 | 24160 | 24159.96 |
| ESE | 0 | 0 | 0 | 0 | 24160 | 24160 | 24160 | 24160 |
| SSE | 0 | 0 | 0 | 0 | 24160 | 24160 | 24159.88 | 24160 |
| S | 0 | 0 | 0 | 0 | 24158.24 | 24152.44 | 24151.24 | 24158.12 |
| SSW | 0 | 0 | 0 | 0 | 22200.56 | 20245.96 | 19530.72 | 22607.52 |
| WSW | 4.115E-05 | 4.30495E-05 | 3.87E-05 | 3.99E-05 | 536 | 363.2 | 296.76 | 642.52 |
| W | 6.693E-05 | 0.000065345 | 6.24E-05 | 5.96E-05 | 624.4 | 715.52 | 724.32 | 1292.32 |
| WNW | 8.804E-05 | 9.03033E-05 | 8.72E-05 | 8.16E-05 | 797.36 | 704.04 | 1179.36 | 1529.12 |
| NNW | 5.529E-05 | 5.44661E-05 | 5.08E-05 | 4.82E-05 | 746.24 | 846.48 | 1315.2 | 1405.12 |
| Weighted total | 2.466E-05 | 2.48849E-05 | 2.33E-05 | 2.27E-05 | 11402.35 | 11278.9 | 11311.95 | 11634.18 |

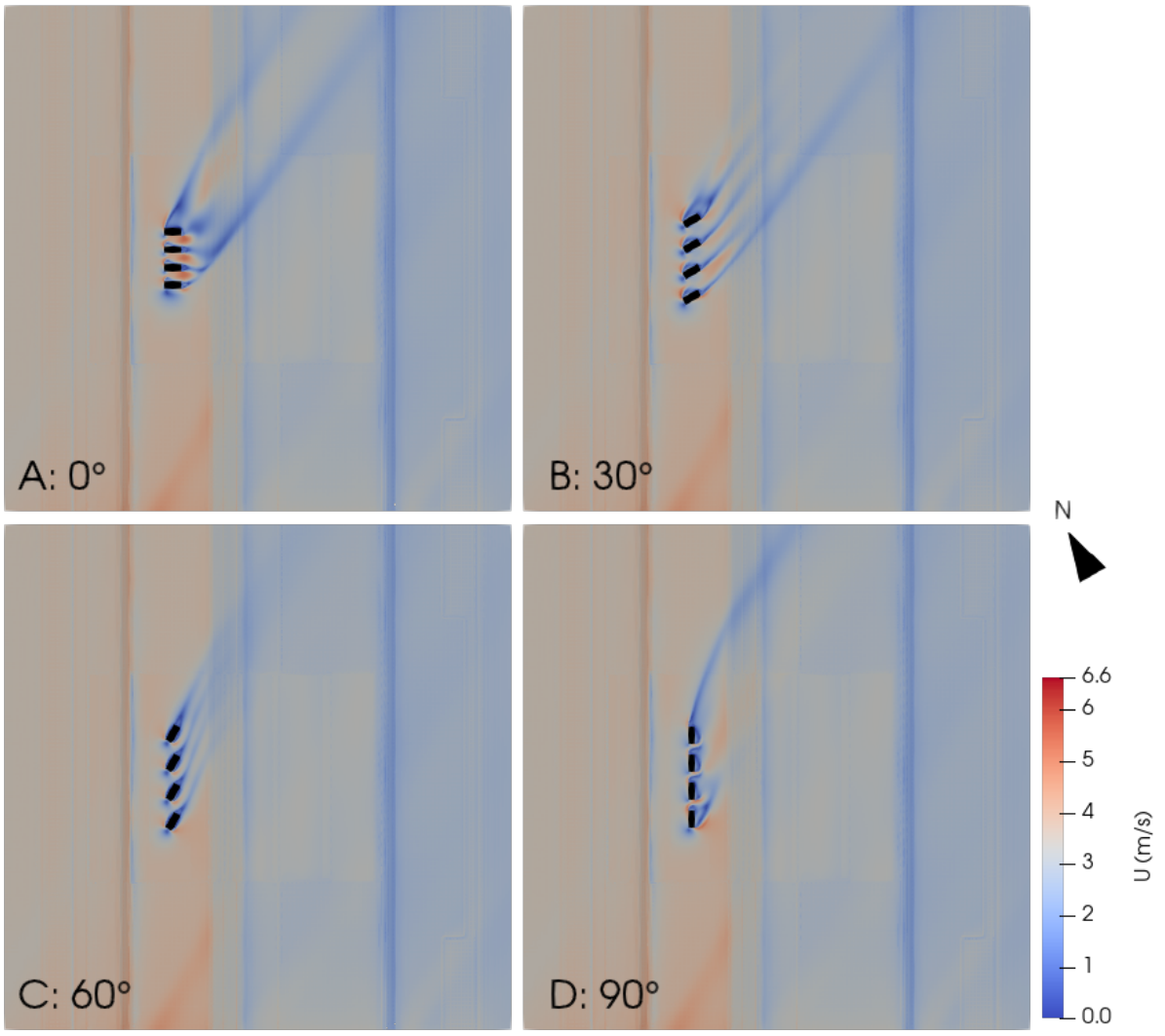


**Figure C.2.** Configurations group 2: wind speed - wind coming from WSW direction

## C.4 Results configuration group 3

**Table C.4.** Results group 3

| Group 3 | *Dune-ward sediment transport (kg/m/s)* | | | | *Area without movement (m2)* | | | |
|---|---|---|---|---|---|---|---|---|
| **Wind direction** | **A** | **B** | **C** | **D** | **A** | **B** | **C** | **D** |
| N | 0 | 0 | 0 | 2.32E-07 | 1728.6 | 2236.64 | 2436.16 | 2087.72 |
| NNE | 0 | 0 | 0 | 0 | 24099.36 | 24117.8 | 24113.36 | 24128.8 |
| ENE | 0 | 0 | 0 | 0 | 24159.96 | 24156.6 | 24159.36 | 24158.32 |
| E | 0 | 0 | 0 | 0 | 24160 | 24160 | 24160 | 24160 |
| ESE | 0 | 0 | 0 | 0 | 24160 | 24160 | 24160 | 24160 |
| SSE | 0 | 0 | 0 | 0 | 24160 | 24160 | 24160 | 24160 |
| S | 0 | 0 | 0 | 0 | 24159.28 | 24151.24 | 24148.04 | 24159.36 |
| SSW | 0 | 0 | 0 | 0 | 20361.92 | 18312.28 | 17727 | 21067.08 |
| WSW | 4.13946E-05 | 4.36867E-05 | 4.1E-05 | 4.16E-05 | 534.64 | 429.4 | 374.96 | 420.32 |
| W | 0.00006671 | 6.50704E-05 | 6.32E-05 | 6.15E-05 | 608.24 | 671.68 | 624.24 | 1051.68 |
| WNW | 8.83909E-05 | 8.91495E-05 | 8.66E-05 | 8.27E-05 | 755.36 | 765.96 | 1333.88 | 1530.12 |
| NNW | 5.58843E-05 | 5.45204E-05 | 4.85E-05 | 4.89E-05 | 825.08 | 1092.44 | 1662.28 | 1672.16 |
| Weighted total | 2.47129E-05 | 2.48865E-05 | 2.35E-05 | 2.32E-05 | 11293.33 | 11200.21 | 11257.1 | 11548.63 |

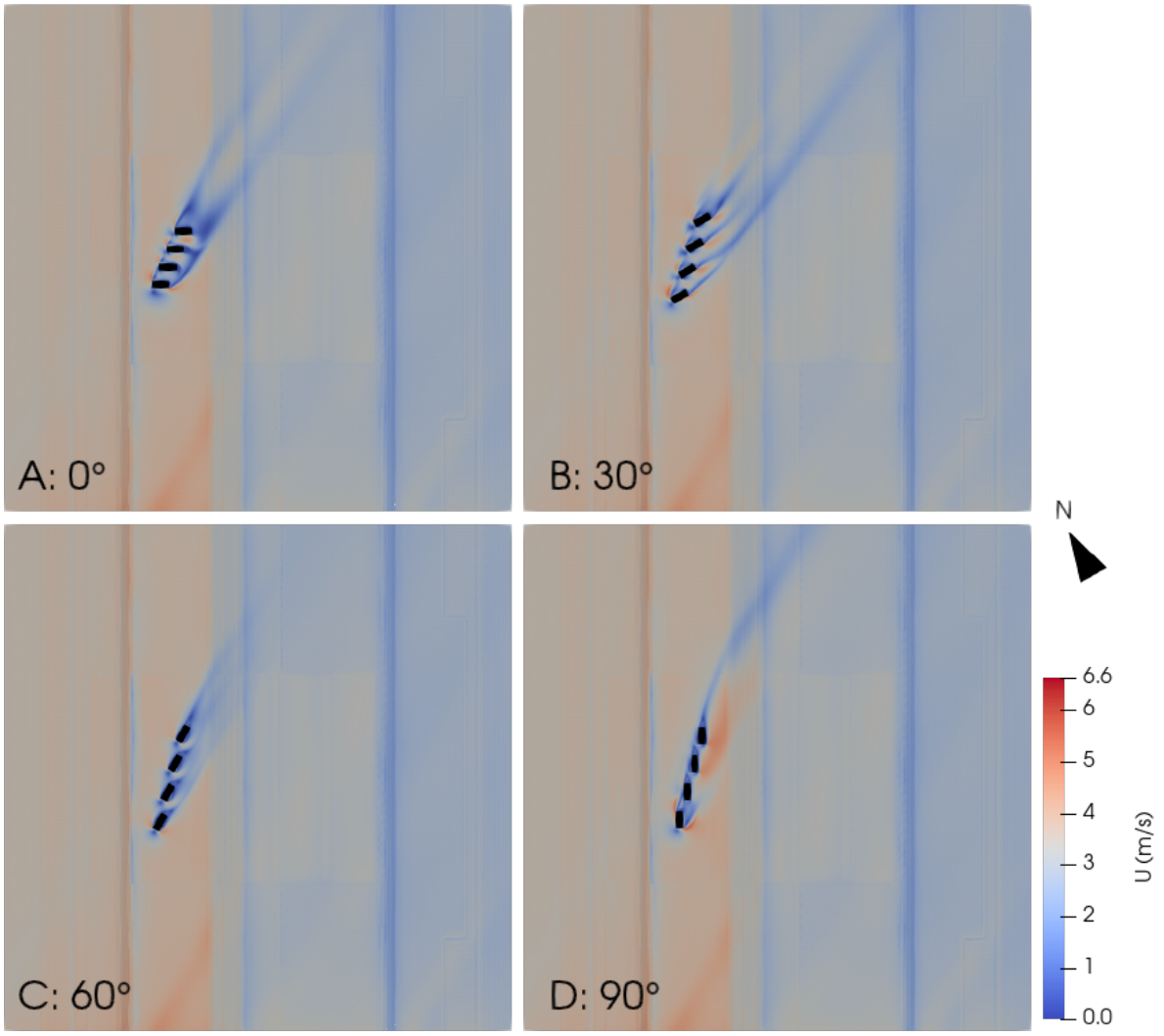


**Figure C.3.** Configurations group 3: wind speed - wind coming from WSW direction

## C.5 Results configuration group 4

**Table C.5.** Results group 4

| Group 4 | *Dune-ward sediment transport (kg/m/s)* | | | *Area without movement (m2)* | | |
|---|---|---|---|---|---|---|
| **Wind direction** | **A** | **B** | **C** | **A** | **B** | **C** |
| N | 0 | 0 | 0 | 1823.96 | 1851.88 | 2203.52 |
| NNE | 0 | 0 | 0 | 24099.28 | 24078 | 24078.28 |
| ENE | 0 | 0 | 0 | 24159.8 | 24158.24 | 24159.72 |
| E | 0 | 0 | 0 | 24159.88 | 24160 | 24159.96 |
| ESE | 0 | 0 | 0 | 24160 | 24160 | 24160 |
| SSE | 0 | 0 | 0 | 24160 | 24160 | 24160 |
| S | 0 | 0 | 0 | 24159.16 | 24157.72 | 24159.88 |
| SSW | 0 | 0 | 0 | 19370.92 | 21602.4 | 19262.48 |
| WSW | 3.97191E-05 | 4.06051E-05 | 4.21E-05 | 845.8 | 753 | 750.44 |
| W | 6.38489E-05 | 6.47014E-05 | 6.52E-05 | 982.28 | 876.36 | 922.64 |
| WNW | 8.69418E-05 | 8.54228E-05 | 8.69E-05 | 1104.72 | 1217.04 | 1102.4 |
| NNW | 5.38045E-05 | 5.12281E-05 | 5.26E-05 | 1109.12 | 1078.04 | 1173.68 |
| Weighted total | 2.38747E-05 | 2.37512E-05 | 2.43E-05 | 11362.89 | 11524.36 | 11380.82 |

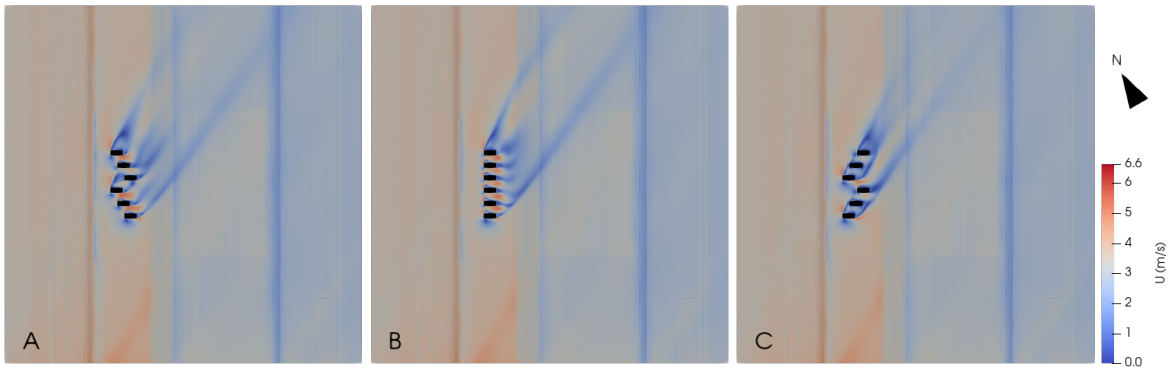


**Figure C.4.** Configurations group 4: wind speed - wind coming from WSW direction

## C.6 Results configuration group 5

**Table C.6.** Results group 5

| Group 5 | *Dune-ward sediment transport (kg/m/s)* | | | *Area without movement (m2)* | | |
|---|---|---|---|---|---|---|
| **Wind direction** | **A** | **B** | **C** | **A** | **B** | **C** |
| N | 0 | 0 | 0 | 2063.6 | 1851.8 | 1965.24 |
| NNE | 0 | 0 | 0 | 24113.04 | 24077.96 | 24111.84 |
| ENE | 0 | 0 | 0 | 24159.32 | 24158.24 | 24159.36 |
| E | 0 | 0 | 0 | 24159.92 | 24160 | 24159.92 |
| ESE | 0 | 0 | 0 | 24160 | 24160 | 24160 |
| SSE | 0 | 0 | 0 | 24160 | 24160 | 24160 |
| S | 0 | 0 | 0 | 24158.72 | 24157.72 | 24158.56 |
| SSW | 0 | 0 | 0 | 20048 | 21602.64 | 19149.28 |
| WSW | 4.09442E-05 | 4.06034E-05 | 4.16E-05 | 752.96 | 752.92 | 764.24 |
| W | 6.47868E-05 | 6.47009E-05 | 6.48E-05 | 947.12 | 876.28 | 920.84 |
| WNW | 8.62925E-05 | 8.54228E-05 | 8.64E-05 | 1187.28 | 1216.96 | 1086.04 |
| NNW | 5.25072E-05 | 5.12277E-05 | 5.3E-05 | 1155.6 | 1078.16 | 1097.64 |
| Weighted total | 2.39984E-05 | 2.37508E-05 | 2.42E-05 | 11437.08 | 11524.35 | 11340.18 |

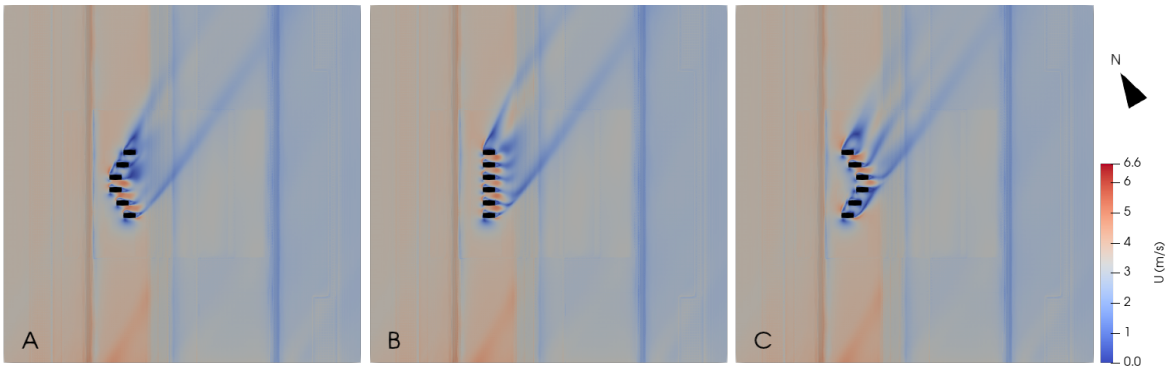


**Figure C.5.** Configurations group 5: wind speed - wind coming from WSW direction

# D

# Reproducibility self-assessment

## D.1 Marks for each of the criteria

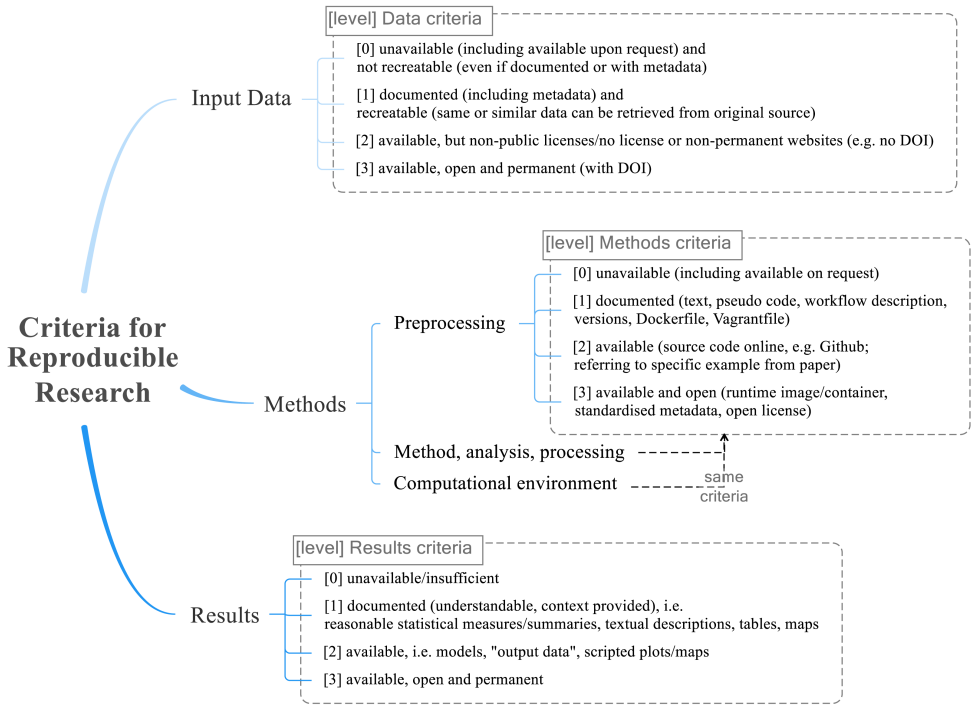


**Figure D.1.** Reproducibility criteria to be assessed.

Grade for the 5 criteria:

1. input data - score: 3. The KNMI data is openly available and easy to access. Metadata including DOI is available too.
2. preprocessing - score: 1. The preprocessing is documented in this thesis.
3. methods - score: 1. The methods are documented, the source code is not published in this thesis completely but available on request.
4. computational environment - score: 3. The software used, (OpenFOAM, Python, PostgreSQL QGIS) is all open-source. The majority work on all platforms, however OpenFOAM is only available trough Linux.
5. results - score: 1-2. The results, including output data, are documented in this thesis. Resulting models are available under request.

# Bibliography


Abraham Kelilo Tula, & Firaol Befikadu Geleta. (2019). Building Urban Land Information Management System in PostgreSQL, for the Case of Ethiopia. *Journal of Communication and Computer*, *15*, 25–37. https://doi.org/10.17265/1548-7709/2019.01.003

Arcadis. (2008). Noordwijk Boulevard. Retrieved January 3, 2021, from https://www.landscape-architects.nl/en/projects/noordwijk-boulevard

Arens, S. M., Mulder, J. P., Slings, Q. L., Geelen, L. H., & Damsma, P. (2013). Dynamic dune management, integrating objectives of nature development and coastal safety: Examples from the Netherlands. *Geomorphology*, *199*, 205–213. https://doi.org/10.1016/j.geomorph.2012.10.034

Bagnold, R. A. (1937). The Transport of Sand by Wind. *The Geographical Journal*, *89*(5), 409–438.

Bagnold, R. A. (1941). *The physics of blown sand and desert dunes* (5th ed.). Chapman & Hall.

Blazek, J. (2005). *Computational Fluid Dynamics: Principles and Applications*. Elsevier Ltd. https://doi.org/10.1016/B978-0-08-044506-9.X5000-0

Blocken, B., Stathopoulos, T., & van Beeck, J. P. (2016). Pedestrian-level wind conditions around buildings: Review of wind-tunnel and CFD techniques and their accuracy for wind comfort assessment. *Building and Environment*, *100*, 50–81. https://doi.org/10.1016/j.buildenv.2016.02.004

Blocken, B. (2014). 50 years of Computational Wind Engineering: Past, present and future. *Journal of Wind Engineering and Industrial Aerodynamics*, *129*, 69–102. https://doi.org/10.1016/j.jweia.2014.03.008

Blocken, B. (2015). Computational Fluid Dynamics for urban physics: Importance, scales, possibilities, limitations and ten tips and tricks towards accurate and reliable simulations. *Building and Environment*, *91*(May), 219–245. https://doi.org/10.1016/j.buildenv.2015.02.015

Blocken, B., Stathopoulos, T., & Carmeliet, J. (2007). CFD simulation of the atmospheric boundary layer: wall function problems. *Atmospheric Environment*, *41*(2), 238–252. https://doi.org/10.1016/j.atmosenv.2006.08.019

Bradshaw, P., & Huang, G. P. (1995). The law of the wall in turbulent flow. *Proceedings - Royal Society of London, A*, *451*(1941), 165–188. https://doi.org/10.1098/rspa.1995.0122

Celik, I. B., Ghia, U., Roache, P. J., Freitas, C. J., Coleman, H., & Raad, P. E. (2008). Procedure for estimation and reporting of uncertainty due to discretization in CFD applications. *Journal of Fluids Engineering, Transactions of the ASME*, *130*(7), 0780011–0780014. https://doi.org/10.1115/1.2960953

Cermak, J. E. (1975). Application of Fluid Mechanics to Wind Engineering - A Freeman Scholar Lecture.

CfMesh. (2021). What is cfMesh? Retrieved April 3, 2021, from https://cfmesh.com/cfmesh/

Chakrabarty, R., & Shih, A. M. (2004). *A Distributed Scientific Data Visualization Framework for CFD Applications*.

Davidson-Arnott, R. G., & Law, M. N. (1996). Measurement and prediction of long-term sediment supply to coastal foredunes. *Journal of Coastal Research*, *12*(3), 654–663.

de Klerk, R. P. (2019). *The influence of buildings on aeolian coastal dune development* (MSc Thesis). TU Delft.

Delgado-Fernandez, I. (2011). Meso-scale modelling of aeolian sediment input to coastal dunes. *Geomorphology*, *130*(3-4), 230–243. https://doi.org/10.1016/j.geomorph.2011.04.001

Delgado-Fernandez, I., & Davidson-Arnott, R. (2011). Meso-scale aeolian sediment input to coastal dunes: The nature of aeolian transport events. *Geomorphology*, *126*(1-2), 217–232. https://doi.org/10.1016/j.geomorph.2010.11.005

Deltaprogramma. (2012). *Werk aan de delta - maatregelen van nu, voorbereiding voor morgen* (tech. rep.). Rijkswaterstaat.

Deltaprogramma. (2020). *Deltaprogramma 2021 Koersvast Werken Aan Een Klimaatbestendig Nederland* (tech. rep.). Rijkswaterstaat.

Deltares. (2017). *Delta scenarios voor de 21e eeuw* (tech. rep.). Deltares.

de Winter, R. C., & Ruessink, B. G. (2017). Sensitivity analysis of climate change impacts on dune erosion: case study for the Dutch Holland coast. *Climatic Change*, *141*(4), 685–701. https://doi.org/10.1007/s10584-017-1922-3

Dillavou, M. W., Shum, P. C., Dorothy, F. W., Shih, A. M., & Soni, B. K. (2008). CaseMan, A CFD case management toolkit. *46th AIAA Aerospace Sciences Meeting and Exhibit*, 1–8. https://doi.org/10.2514/6.2008-928

Eymard, R., Gallouët, T., & Raphaèle, H. (2019). Finite volume methods. https://doi.org/10.1007/978-3-319-99693-6_4

Franke, J., Hellsten, A., Schlünzen, H., & Carissimo, B. (2007). *Best practice guideline for the CFD simulation of flows in the urban environment*. COST Office.

García-Sánchez, C., Van Tendeloo, G., & Gorlé, C. (2017). Quantifying inflow uncertainties in RANS simulations of urban pollutant dispersion. *Atmospheric Environment*, *161*, 263–273. https://doi.org/10.1016/j.atmosenv.2017.04.019

Gregorio, F. D., & Varrazzo, D. (2021). Psycopg – PostgreSQL database adapter for Python. https://www.psycopg.org/docs/

Grootjans, A. P., Geelen, H. W., Jansen, A. J., & Lammerts, E. J. (2002). Restoration of coastal dune slacks in the Netherlands. *Hydrobiologia*, *478*, 181–203. https://doi.org/10.1023/A:1021086832201

Haasnoot, M., Mosselman, E., Sloff, K., Huismans, Y., Mens, M., Ter Maat, K., Weiler, O., Bouwer, L., Diermanse, F., Kwadijk, J., Van der Spek, A., Oude Essink, G., & Delsman, J. (2018). *Mogelijke gevolgen van versnelde zeespiegelstijging voor het Deltaprogramma* (tech. rep.). Deltares.

Hirsch, C. (2007). *Numerical Computation of Internal and External Flows: The Fundamentals of Computational Fluid Dynamics* (Second Edi). Butterworth-Heinemann. https://doi.org/10.1016/B978-0-7506-6594-0.X5037-1

Hoonhout, B., & van Thiel de Vries, J. (2013). *Invloed van strandbebouwing op zandverstuiving* (tech. rep.). Deltares.

Jackson, N. L., & Nordstrom, K. F. (2011). Aeolian sediment transport and landforms in managed coastal systems: A review. *Aeolian Research*, *3*, 181–196. https://doi.org/10.1016/j.aeolia.2011.03.011

KNMI. (2019). Wind - model time series from 2014 to august 2019 at 10-200 meters above the north sea in individual 2.5 km grid location files. Retrieved April 25, 2021, from https://dataplatform.knmi.nl/catalog/datasets/index.html?x-dataset=KNW-CSV-TS-UPDATE%7B%5C&%7Dx-dataset-version=1.0

KNMI. (2021). KNMI Data Platform. Retrieved April 18, 2021, from https://dataplatform.knmi.nl/

Lamberti, G., García-Sánchez, C., Sousa, J., & Gorlé, C. (2018). Optimizing turbulent inflow conditions for large-eddy simulations of the atmospheric boundary layer. *Journal of Wind Engineering and Industrial Aerodynamics*, *177*, 32–44. https://doi.org/10.1016/j.jweia.2018.04.004

Li, F., van Gelder, P., Callaghan, D., Jongejan, R., Heijer, C., & Ranasinghe, R. (2013). Probabilistic modeling of wave climate and predicting dune erosion. *Journal of Coastal Research*, *65*, 760–765. https://doi.org/10.2112/si65-129.1

Mandal, B. C., & Mazumdar, H. P. (2015). The importance of the law of the wall. *International Journal of Applied Mechanics and Engineering*, *20*(4), 857–869. https://doi.org/10.1515/ijame-2015-0055

Murakami, S., & Mochida, A. (1989). Three-dimensional numerical simulation of turbulent flow around buildings using the k-$\epsilon$ turbulence model. *Building and Environment*, *24*(1), 51–64. https://doi.org/10.1016/0360-1323(89)90016-4

Nieuwstadt, F., & Duynkerke, P. (1996). Turbulence in the Atmospheric Boundary Layer. *Atmospheric Research*, *40*, 111–142.

Nordstrom, K. F., & Jackson, N. L. (2013). Foredune restoration in Urban Settings. *Springer Series on Environmental Management*. https://doi.org/10.1007/978-3-642-33445-0

OpenCFD Ltd. (2016). About OpenFOAM. Retrieved April 3, 2021, from http://www.openfoam.com/

Pieterse, J. E., & Harms, T. M. (2013). CFD investigation of the atmospheric boundary layer under different thermal stability conditions. *Journal of Wind Engineering and Industrial Aerodynamics*, *121*, 82–97. https://doi.org/10.1016/j.jweia.2013.07.014

Pourteimouri, P., Campmans, G., Wijnberg, K., & Hulscher, S. (2020). The impact of buildings' characteristics on airflow patterns and bed morphology at beaches, using CFD modelling. *Coastal Engineering Proceedings*, (October), 3–7.

Presley, D., & Tatarko, J. (2009). Principles of Wind Erosion and its Control. *Kansas State University Research and Extension*.

Richards, P. J., & Hoxey, R. P. (1993). Appropriate boundary conditions for computational wind engineering models using the k-ε turbulence model. *Journal of Wind Engineering and Industrial Aerodynamics*, *46-47*(100), 145–153. https://doi.org/10.1016/0167-6105(93)90124-7

Rijkswaterstaat. (1990). *A new coastal defence policy for the Netherlands* (tech. rep.). Rijkswaterstaat.

Rijkswaterstaat. (2009). Suppletie Vlissingen. Retrieved January 14, 2021, from https://beeldbank.rws.nl

Rijkswaterstaat. (2017). *Kustpact* (tech. rep.). Rijkswaterstaat.

Rijkswaterstaat. (2021). Kustonderhoud: waar werken we. Retrieved May 10, 2021, from https : / / www . rijkswaterstaat . nl / water / waterbeheer / bescherming - tegen - het - water / maatregelen - om - overstromingen-te-voorkomen/kustonderhoud/waar-werken-we%7B%5C#%7D2662591

Sherman, D. J., & Li, B. (2012). Predicting aeolian sand transport rates: A reevaluation of models. *Aeolian Research*, *3*(4), 371–378. https://doi.org/10.1016/j.aeolia.2011.06.002

Sherman, D. J., Li, B., Ellis, J. T., Farrell, E. J., Maia, L. P., & Granja, H. (2013). Recalibrating aeolian sand transport models. *Earth Surface Processes and Landforms*, *38*(2), 169–178. https://doi.org/10.1002/esp.3310

Stronkhorst, J., Huisman, B., Giardino, A., Santinelli, G., & Santos, F. D. (2018). Sand nourishment strategies to mitigate coastal erosion and sea level rise at the coasts of Holland (The Netherlands) and Aveiro (Portugal) in the 21st century. *Ocean and Coastal Management*, *156*(November), 266–276. https://doi.org/10.1016/j.ocecoaman.2017.11.017

Toimil, A., Losada, I. J., Nicholls, R. J., Dalrymple, R. A., & Stive, M. J. (2020). Addressing the challenges of climate change risks and adaptation in coastal areas: A review. *Coastal Engineering*, *156*(July 2019). https://doi.org/10.1016/j.coastaleng.2019.103611

Tominaga, Y., Mochida, A., Yoshie, R., Kataoka, H., Nozu, T., Yoshikawa, M., & Shirasawa, T. (2008). AIJ guidelines for practical applications of CFD to pedestrian wind environment around buildings. *Journal of Wind Engineering and Industrial Aerodynamics*, *96*(10-11), 1749–1761. https://doi.org/10.1016/j.jweia.2008.02.058

Tu, J., Yeoh, G.-H., & Liu, C. (2018a). CFD Mesh Generation: A Practical Guideline. *Computational fluid dynamics* (pp. 125–154). Elsevier Ltd. https://doi.org/10.1016/b978-0-08-101127-0.00004-0

Tu, J., Yeoh, G.-H., & Liu, C. (2018b). Practical Guidelines for CFD Simulation and Analysis. *Computational fluid dynamics* (pp. 255–290). Elsevier Ltd. https://doi.org/10.1016/b978-0-08-101127-0.00007-6

van Bergen, J., Mulder, J., Nijhuis, S., Poppema, D., Wijnberg, K., & Kuschnerus, M. (2021). Urban dunes towards BwN design principles for dune formation along urbanized shores. *Research in Urbanism Series*, *7*, 101–127. https://doi.org/10.47982/rius.7.130

van Bergen, J., & Nijhuis, S. (2019). ShoreScape : Nature-Based Design for Urban Coastal Zones. *Coastal Management 2019*, 319–332. https://doi.org/https://doi.org/10.1680/cm.65147.319

van Onselen, E. (2018). *Analysing measures to improve beach - dune interaction in the presence of man - made structures using computational fluid dynamics ( CFD )* (MSc Thesis). Utrecht University.

van Rijn, L. (2011). Coastal erosion and control. *Ocean and Coastal Management*, *54*(12), 867–887. https://doi.org/10.1016/j.ocecoaman.2011.05.004

van Rijn, L. C. (2019). *Aeolian transport over a flat sediment surface* (tech. rep.). -. leovanrijn-sediment.com

van Westen, B. (2019). *Invloed strandbebouwing op duinontwikkeling* (tech. rep.). Deltares.

Yu, J. J., Qin, X. S., Larsen, L. C., Larsen, O., Jayasooriya, A., & Shen, X. L. (2012). A GIS-based management and publication framework for data handling of numerical model results. *Advances in Engineering Software*, *45*(1), 360–369. https://doi.org/10.1016/j.advengsoft.2011.10.010

## Colophon

This document was typeset using LaTeX, using the `book` class.
Diagrams are made using https://app.diagrams.net/, icons downloaded from https://icons8.com/
Results from the CFD simulations are shown using ParaView, https://www.paraview.org/


TUDelft